Journal of Water Resources and Ocean Science
2026, Vol. 15, No. 3, pp. 106–142
https://doi.org/10.11648/j.wros.20261503.15

Research Article

Spatial Interpolation of Hydrographic Vertical References in the Gulf of Guinea: Hierarchical Ranking of Geostatistical and Deterministic Methods by LOO Cross-validation

Michel Mfeze*

National Advanced School of Engineering, University of Yaounde I, Yaounde, Cameroon

Abstract

The accurate determination of the offset between Mean Sea Level (MSL) and Lowest Astronomical Tide (LAT) is very important for marine and coastal navigation, mapping, and engineering (reduction of bathymetric soundings to LAT, under-keel clearance, and nearshore/offshore infrastructure levelling). The MSL value is obtained from either a local geoid model or from temporary in-situ tide gauge data processed using specialised filters. For many ungauged ports along the Gulf of Guinea, sources like Admiralty Tide Tables (ATT) provide insufficient spatial coverage, necessitating spatial interpolation from regional reference gauges. The low density, heterogeneity, and discontinuity of tide gauge observations impose the use of rigorously evaluated spatial interpolation methods. This study proposes an integrated methodological framework comparing six interpolation techniques: Nearest Neighbour (NN), Inverse-Distance Weighting (IDW), Triangulation (TIN), Spline, Trend Surface, and Kriging. The comparison is based on a regional database of 115 reference ports (106 from the ATT, and nine complementary stations from GLOSS, PSMSL, and UHSLC/JASL networks) spanning 20 West African coastal countries. Three representative Cameroonian test sites are selected: the Rio del Rey Shelf (Betika), the Wouri Estuary (Dibamba-Yassa), and the isolated southern coast (Batanga). The approach combines a unified software implementation, exhaustive comparison and leave-one-out (LOO) cross-validation (MAE, RMSE, bias, R^2), convergence analysis and quadratic decomposition of uncertainty components. Results indicate that the optimal interpolation method varies with local reference station density and spatial configuration. At Betika (18 reference stations, 9 retained), IDW yields the best cross validation performance (RMSE ≈ 0.2295 m, R^2 ≈ 0.1376) with Kriging close behind. At Dibamba-Yassa (06 stations, 4 retained), Trend Surface performs best (RMSE ≈ 0.1225 m, R^2 ≈ 0.2833), followed by Kriging (RMSE=0.1439 m). At Batanga (2 stations only), method comparison fails, illustrating problem degeneration under extreme undersampling. In all cases, interpolation variance σ_i^2 accounts for more than 95% of the total error budget, with 95% confidence intervals reaching ±3.6 m to ±4.9 m. The convergence analysis shows that a minimum of 5-7 stations is required to stabilise estimates. The main finding is that network densification is the primary lever for improvement, well ahead of algorithmic optimisation. The study provides validated point estimates for the three sites and a transparent protocol for tidal datum estimation in data sparse coastal regions of the Gulf of Guinea.

Keywords

Deterministic Method, Geostatistical Method, Hydrography, LOO Cross-validation, MSL-LAT, Spatial Interpolation, Uncertainty, Vertical Reference

*Correspondence: Michel Mfeze (mfeze@yahoo.fr)

Received: 4 June 2026; **Accepted:** 16 June 2026; **Published:** 30 June 2026

1. Introduction

The MSL-LAT differential is a fundamental requirement for marine mapping, navigation safety, and coastal/offshore engineering [1]. This offset governs bathymetric sounding reduction, under-keel clearance monitoring, and infrastructure levelling. It is not spatially uniform, governed by local hydrodynamic, bathymetric, and astronomical processes [2]. Accurate realisation of the LAT surface requires combining hydrodynamic model-derived estimates with tide gauge observations [3].

Where geoid models are unavailable or of insufficient accuracy [4], MSL is estimated from in-situ tide gauge data processed with specialised filters (Doodson X0, Godin, Demerliac) [5]. The MSL-LAT differential is then drawn from datasets such as the Admiralty Tide Tables (ATT) [6], whose spatial coverage remains limited. This constraint is particularly critical along West African coasts: the tide gauge network is heterogeneous and sparse [7, 8]. Sea level datasets are limited in size and quality [9, 10], with tidal regimes spanning microtidal (~0.76 m in Ghana) to macrotidal (>3.9 m in Guinea-Bissau) [11]. To address these coverage gaps, this study enriches the 106-station ATT database with 9 complementary stations drawn from internationally validated databases (GLOSS, PSMSL, UHSLC/JASL) spanning the northern West African coast from Cape Verde to Mauritania. Spatial interpolation is therefore indispensable for uninstrumented coastal sites in the Gulf of Guinea.

Interpolation reliability depends strongly on the spatial configuration, density, and distribution of reference stations, requiring both non-stationarity representation and robust uncertainty quantification [12, 13].

Turner et al. [14] showed that tidal levels including LAT and MSL can vary significantly over short distances in estuarine settings, making interpolation method and station distribution critical factors. Orton et al. [15] found IDW and Kriging suitable for regional tide datum interpolation in well-gauged regions; their applicability to sparse Gulf of Guinea networks has not been systematically validated. Previous practice has relied on ad hoc nearest-neighbour assignments or graphical interpolation from Admiralty Tables, without spatial gradient correction or IHO M-3 uncertainty quantification [16]. In contrast, advanced methodologies such as hydrographic vertical separation surfaces (HyVSEPs) [17], demonstrate achievable accuracy when network density and modelling tools are combined, highlighting the gap that persists in undersampled regions like the Gulf of Guinea. The vertical datum uncertainties arising from such simplified approaches can be substantial, compromising hydrographic survey quality and maritime safety [18].

Existing methods fall into three families [19]: deterministic (NN, IDW, TIN, Spline), geostatistical (Kriging [20]), and hybrid approaches. Inter-method discrepancies can reach 0.5 m in certain regions [11], incompatible with IHO S-44 hydrographic survey precision. Despite this methodological diversity, comparative evaluations remain rare in this specific context of African coasts although satellite altimetry offers complementary sea-level observations that can partially compensate for the sparse tide gauge coverage in the region [21, 22].

These limitations raise several major operational questions: which interpolation method yields the most reliable estimates under sparse and heterogeneous data? What is the optimal number of neighbouring stations guaranteeing estimate convergence? How can total uncertainty, from data, interpolation processes, and modelling assumptions, be rigorously quantified and propagated?

To address these challenges, this study proposes an integrated framework for comparative evaluation of spatial interpolation methods applied to hydrographic vertical references, based on: (i) an enriched 115-port regional database spanning 20 countries; (ii) unified Java implementation of six algorithms (NN, IDW, TIN, Spline, Trend Surface, Kriging); (iii) systematic leave-one-out (LOO) cross-validation (MAE, RMSE, bias, R^2); (iv) convergence analysis; (v) quadratic uncertainty decomposition; and (vi) application to three Cameroonian sites representative of principal hydrographic configurations in the Gulf of Guinea.

Beyond algorithmic comparison, this framework provides a decision-support tool for hydrographic services, enabling objective method selection, transparent reliability evaluation, and guidance for tide gauge network densification strategies. By establishing an explicit link between method performance and spatial data configuration, this study contributes to improving the reliability and harmonisation of vertical reference systems in undersampled coastal regions, in service of maritime safety and the blue economy [23].

2. Materials and Methods

2.1. Regional Hydrographic Context of the Gulf of Guinea

The Gulf of Guinea presents a semi-diurnal mesotidal regime; M_2 accounts for >96% of sea-level variance in the Wouri Estuary [5, 24]. Mean tidal range varies from microtidal at Takoradi (0.76 m) and Lagos (0.78 m) to mesotidal in Cameroon and Nigeria, peaking at Calabar (≈2.09 m) and Douala (≈1.62 m) [25]. These spatial contrasts reflect the influence of seasonal upwelling and regional hydrodynamic forcing documented across the Gulf of Guinea [26].

Nine complementary stations from GLOSS/ PSMSL/ UHSLC provide spatial anchoring for the northern domain. Dakar hosts one of Africa's longest sea level records [8, 27, 28]. Palmeira and Nouakchott document sea level rise of 4.51 and 20.08 mm/year respectively [29]. Δ_i values are derived from FES2014 harmonic model with estimated uncertainty ±0.10-0.15 m.

2.2. Spatial Interpolation Database

The database comprises 115 ports across 20 West African countries (Figure 1, Table 1). 106 are from the Admiralty Tide Tables [6]; 9 complementary stations from GLOSS/PSMSL/UHSLC. Each entry P_i includes coordinates (ϕ_i, λ_i, WGS84), MSL-LAT differential Δ_i, and tidal regime Ti.

$$P_i = \{ N_i, C_i, S_i, \phi_i, \lambda_i, \Delta_i, T_i \} \quad (1)$$

Where N_i is the number, C_i is the country, S_i is the station/port, ϕ_i and λ_i are geodetic coordinates (latitude and longitude respectively in WGS84, decimal degrees), Δ_i is the observed MSL-LAT differential (m), and T_i is the tidal regime classification (microtidal/mesotidal/macrotidal). The full dataset is provided in Table 1.

The Gulf of Guinea network has inter-station spacings of 20-200 km [9]. Major ports are 200-500 km apart; local densifications exist around Bonny-Calabar, Douala-Kribi, and Guinea-Bissau islands.

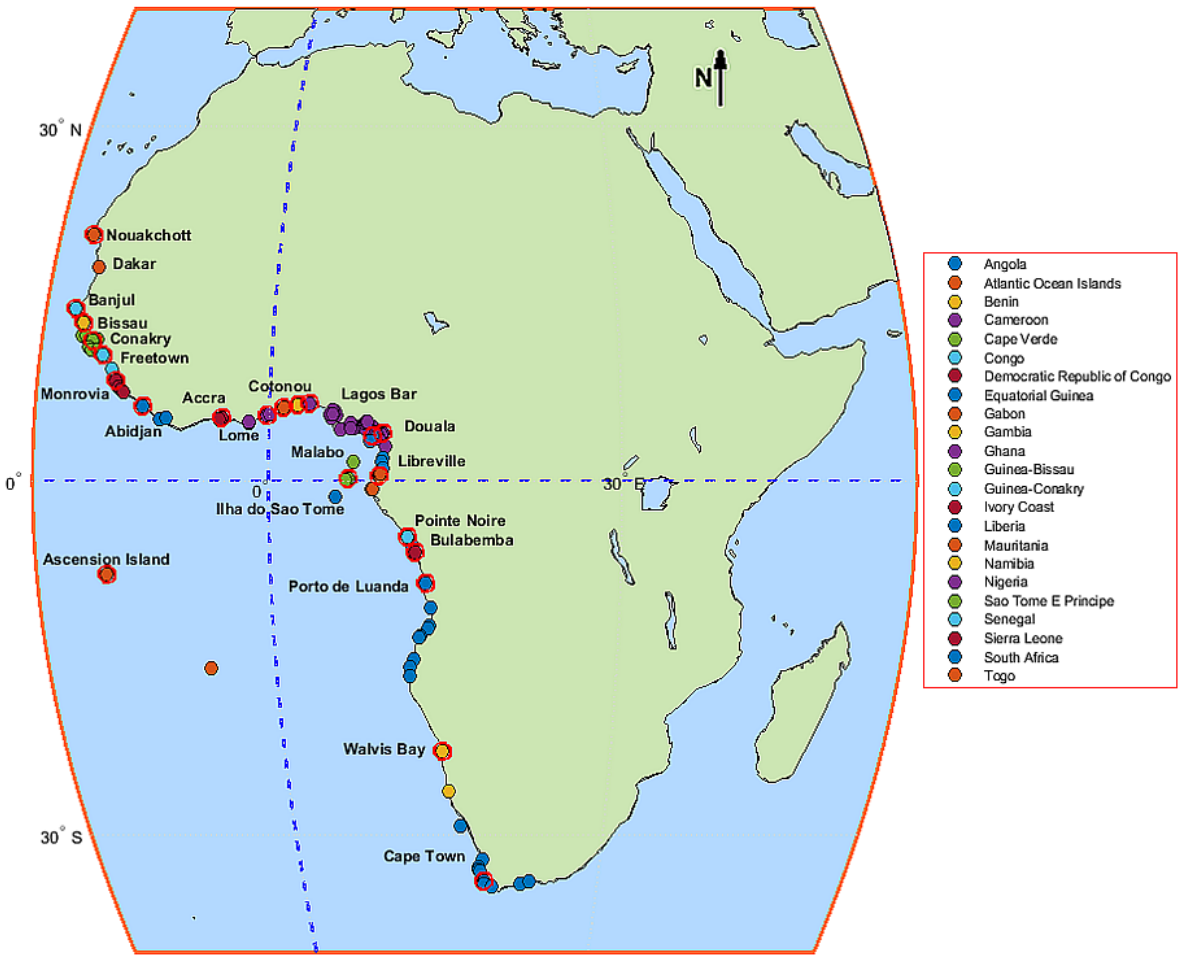

Figure 1. *Spatial distribution of the 115 reference ports across 20 West African coastal countries. Full data Table in Table 1.*

Reliable interpolation is feasible within 20-100 km radii; longer distances (e.g. Lagos-Douala, ~800 km) require hybrid model approaches [24]. Coastal altimetry offers valuable complements for undersampled zones [30].

Table 1. *Reference Ports: MSL-LAT Differential Data.*

No.	Country	Station	ϕ_i (°)	λ_i (°)	Δ_i (m)	T_i[1]
Stations from Admiralty Tide Tables						

[1] Tidal regime classification T_i follows Davies (1964) [42], applied to mean spring tidal range (HAT–LAT) from ATT sources; Δ_i denotes the MSL-LAT differential only.

No.	Country	Station	ϕ_i (°)	λ_i (°)	Δ_i (m)	T_i1
1	Angola	Enseada Cabinda	-5.5500	12.2000	1.10	Micro
2	Angola	Soyo (Santo Ant.)	-6.1167	12.3667	1.10	Micro
3	Angola	Porto de Luanda	-8.7500	13.2500	1.10	Micro
4	Angola	Porto Amboim	-10.7333	13.7167	1.10	Micro
5	Angola	Porto Lobito	-12.3333	13.5667	1.10	Micro
6	Angola	Porto de Benguela	-12.5667	13.4167	0.92	Micro
7	Angola	Baia dos Elefantes	-13.2167	12.7333	1.10	Micro
8	Angola	Baia de Santa M.	-13.3500	12.6500	1.10	Micro
9	Angola	Namibe	-15.2000	12.1500	1.10	Micro
10	Angola	Porto Alexandre	-15.8000	11.8500	1.10	Micro
11	Angola	Baia dos Tigres	-16.6000	11.8167	1.10	Micro
12	Atlantic Is.	Ascension Island	-7.9167	-14.0333	0.70	Micro
13	Atlantic Is.	Saint Helena Is.	-15.9167	-5.7000	0.50	Micro
14	Benin	Cotonou	6.3473	2.4105	0.93	Micro
15	Cameroon	Rio Del Rey Ent.	4.5000	8.8500	1.41	Micro
16	Cameroon	Man O War Bay	3.9667	9.3670	1.20	Micro
17	Cameroon	Entrance Bimbia	4.0667	9.1170	1.10	Micro
18	Cameroon	Tiko-Bimbia R.	4.0500	9.2170	1.20	Micro
19	Cameroon	Cap Cameroun	3.9000	9.4500	1.40	Micro
20	Cameroon	Douala	4.0333	9.7000	1.62	Micro
21	Cameroon	Manoka	3.9167	9.6000	1.42	Micro
22	Cameroon	Malimba	3.5333	9.3833	1.32	Micro
23	Cameroon	Kribi	2.9167	9.9333	1.00	Micro
24	Congo	Pointe Noire	-4.7886	11.8329	0.96	Micro
25	DR Congo	Bulabemba	-6.0500	12.4500	1.00	Micro
26	Eq. Guinea	Pagalu (Annobon)	-1.4167	5.6333	0.80	Micro
27	Eq. Guinea	Bata	1.8667	9.7667	1.02	Micro
28	Eq. Guinea	Rio Benito	1.5667	9.6333	0.96	Micro
29	Eq. Guinea	Cogo-Rio Muni	1.0833	9.7000	1.49	Micro
30	Eq. Guinea	Malabo	3.7500	8.7833	1.16	Micro
31	Eq. Guinea	Bahia de Luba	3.2833	8.5833	1.02	Micro
32	Gabon	Libreville	0.3833	9.4500	1.29	Micro
33	Gabon	Pointe Owendo	0.2886	9.5101	1.45	Micro
34	Gabon	Port Gentil	-0.7149	8.7852	1.45	Micro
35	Gabon	Cap Esterias	0.6167	9.5000	1.40	Micro
36	Gabon	Cap Lopez	-0.6827	8.8580	1.23	Micro
37	Ghana	Takoradi	4.8869	-1.7401	0.76	Micro
38	Ghana	Sekondi	4.9534	-1.7369	0.98	Micro

No.	Country	Station	ϕ_i (°)	λ_i (°)	Δ_i (m)	T_i1
39	Ghana	Accra	5.5599	-0.1964	0.98	Micro
40	Ghana	Tema	5.6579	0.0260	0.88	Micro
41	Guinea-Conakry	Rio Nunez App.	10.6638	-14.5844	2.65	Meso
42	Guinea-Conakry	Port Kamsar	10.6638	-14.5845	3.03	Meso
43	Guinea-Conakry	Conakry	9.5102	-13.7158	2.07	Meso
44	Guinea-Bissau	Varela	12.2865	-16.5949	1.33	Micro
45	Guinea-Bissau	Cacheu	12.2746	-16.1632	1.60	Micro
46	Guinea-Bissau	Ilheu de Caio	12.2794	-16.1655	1.90	Micro
47	Guinea-Bissau	Ponta Biombo	11.7407	-15.9516	2.33	Meso
48	Guinea-Bissau	Bissau	11.8600	-15.5767	2.89	Meso
49	Guinea-Bissau	Jabada	11.9467	-15.3477	3.34	Meso
50	Guinea-Bissau	Porto Gole	11.9668	-15.1347	3.95	Meso
51	Guinea-Bissau	Bolama	11.5772	-15.4798	2.88	Meso
52	Guinea-Bissau	Sanincha	11.8599	-15.5767	2.90	Meso
53	Guinea-Bissau	Bubaque	11.3000	-15.8272	2.54	Meso
54	Guinea-Bissau	João Vieira	11.1333	-15.6318	2.59	Meso
55	Guinea-Bissau	Cacine	11.1318	-15.0233	3.31	Meso
56	Ivory Coast	Abidjan Entrance	5.3327	-4.0296	0.74	Micro
57	Liberia	Monrovia	6.3440	-10.7930	0.90	Micro
58	Liberia	Balfu Bay	5.1529	-9.2901	0.73	Micro
59	Liberia	Sinoe Bay	5.2901	-8.8153	0.91	Micro
60	Namibia	Walvis Bay	-22.9500	14.4833	0.98	Micro
61	Namibia	Luderitz	-26.3167	15.0167	0.94	Micro
62	Nigeria	Warri	5.5499	5.7671	1.04	Micro
63	Nigeria	Forcados River	5.3700	5.4399	0.97	Micro
64	Nigeria	Opobo River	4.5147	7.5284	1.10	Micro
65	Nigeria	Kwa Ibo River	4.6660	7.9884	1.13	Micro
66	Nigeria	Bonny Town	4.4383	7.1592	1.48	Micro
67	Nigeria	Bonny River Bar	4.4296	7.1956	1.43	Micro
68	Nigeria	No 2 Buoy	4.3833	8.4000	1.10	Micro
69	Nigeria	Bakassi Bank	4.4500	8.4000	1.22	Micro
70	Nigeria	Jamestown	4.4833	8.1170	1.48	Micro
71	Nigeria	James Island	4.8667	8.1170	1.34	Micro
72	Nigeria	Calabar	4.9667	8.3170	2.09	Meso
73	Nigeria	Inikoi Island	4.8500	8.3833	1.60	Micro
74	Nigeria	Lagos Bar	6.5255	3.3785	0.78	Micro
75	Nigeria	Badagry Creek	6.4244	3.2440	0.61	Micro
76	Nigeria	Jamestown (2)	5.0167	8.3833	1.48	Micro

No.	Country	Station	ϕ_i (°)	λ_i (°)	Δ_i (m)	T_i1
77	Nigeria	James Island (2)	5.5187	5.7498	1.54	Micro
78	Nigeria	Ogidigbe	5.5558	5.1822	0.97	Micro
79	Nigeria	Forcados	5.3456	5.3463	0.82	Micro
80	Nigeria	Akassa	4.3222	6.0625	0.98	Micro
81	Nigeria	Bonny River	4.4769	7.1744	1.48	Micro
82	Nigeria	Ford Point	4.8027	7.0018	1.52	Micro
83	Nigeria	Port Harcourt	4.8478	6.9650	1.46	Micro
84	Nigeria	Sapele	5.8964	5.6715	0.91	Micro
85	Nigeria	Apapa	6.4574	3.3644	0.88	Micro
86	Nigeria	Youngtown	4.4544	6.9905	0.59	Micro
87	Nigeria	Koko	5.9993	5.4460	0.56	Micro
88	Nigeria	Madagho	5.6019	5.2301	0.86	Micro
89	Nigeria	Rugged Point	5.5827	5.3727	0.75	Micro
90	Sao Tome & Pr.	Ilha do Principe	1.6000	7.2500	1.20	Micro
91	Sao Tome & Pr.	Ilha do Sao Tome	0.2167	6.7500	1.20	Micro
92	Sierra Leone	Freetown	8.4844	-13.2344	1.77	Micro
93	Sierra Leone	Shenge Point	7.9007	-12.9408	1.65	Micro
94	Sierra Leone	Sheather Rock	7.7513	-12.7971	1.68	Micro
95	Sierra Leone	Bonthe	7.5312	-12.5014	0.92	Micro
96	South Africa	Port Nolloth	-29.2500	16.0833	1.09	Micro
97	South Africa	Lamberts Bay	-32.0833	18.3333	0.85	Micro
98	South Africa	Saint Helena Bay	-32.7333	17.8333	0.90	Micro
99	South Africa	Saldanha	-33.0323	17.9214	0.99	Micro
100	South Africa	Schrywershoek	-33.0615	18.0419	0.98	Micro
101	South Africa	Cape Town	-33.9242	18.4127	0.98	Micro
102	South Africa	Simons Town	-34.1929	18.4379	1.00	Micro
103	South Africa	Hermanus	-34.4166	19.2453	1.02	Micro
104	South Africa	Mossel Bay	-34.1837	22.1267	1.17	Micro
105	South Africa	Knysna	-34.0309	23.0226	1.06	Micro
106	Togo	Lome	6.1284	1.2213	1.15	Micro
Complementary Stations - GLOSS / PSMSL / UHSLC2 - ATT3						
107	Senegal	Dakar	14.6333	-17.4500	0.82	Micro
108	Mauritania	Nouakchott	18.0830	-15.9800	0.97	Micro
109	Mauritania	Nouadhibou (Port-Etienne)	20.9000	-17.0500	1.00	Micro
110	Gambia	Banjul	13.4500	-16.5700	1.05	Micro
111	Ivory Coast	Abidjan (GLOSS)	5.2500	-4.2500	0.74	Micro

[2] Complementary stations sourced from GLOSS [8], PSMSL [27], UHSLC/JASL [9]. Δ_i values derived from FES2014/AVISO harmonic amplitudes or PSMSL-UHSLC catalogues (uncertainty ±0.10–0.15 m, k=1)

[3] Admiralty Tide Tables NP203 [6] secondary ports.

No.	Country	Station	ϕ_i (°)	λ_i (°)	Δ_i (m)	T_i1
112	Cameroon	Port Sonara (Limbe)	4.0050	9.1250	1.20	Micro
113	Congo	Pointe Noire (GLOSS)	-4.7830	11.8330	0.96	Micro
114	Sao Tome & Pr.	Sao Tome (PSMSL)	0.0167	6.5167	1.20	Micro
115	Cape Verde	Palmeira (Sal)	16.7550	-22.9300	0.65	Micro

2.3. Selection and Rationale of the Test Sites

Three Cameroonian sites were selected: Dibamba-Yassa, Betika, and Batanga (Table 2, Figure 2). This selection covers the diversity of hydrographic contexts in the Gulf of Guinea enabling a comprehensive evaluation of interpolation methods.

Dibamba-Yassa (Wouri Estuary, <20 m depth) presents a semi-diurnal mesotidal regime with strong fluvial dynamics and low MSL-LAT gradients, testing method robustness where local hydrodynamics dominate.

Betika (Rio del Rey Shelf, 20-50 m depth) presents regular oceanic dynamics and moderate regional MSL-LAT variability, with adequate data density for testing geostatistical method efficacy.

Batanga (Southern Cameroon) illustrates the problem of open coastal zones with simple bathymetry but severely undersampled networks. Very low tide gauge density and large distances to reference stations pose a primarily geometric rather than statistical problem, testing algorithm behaviour under extreme subgrid conditions.

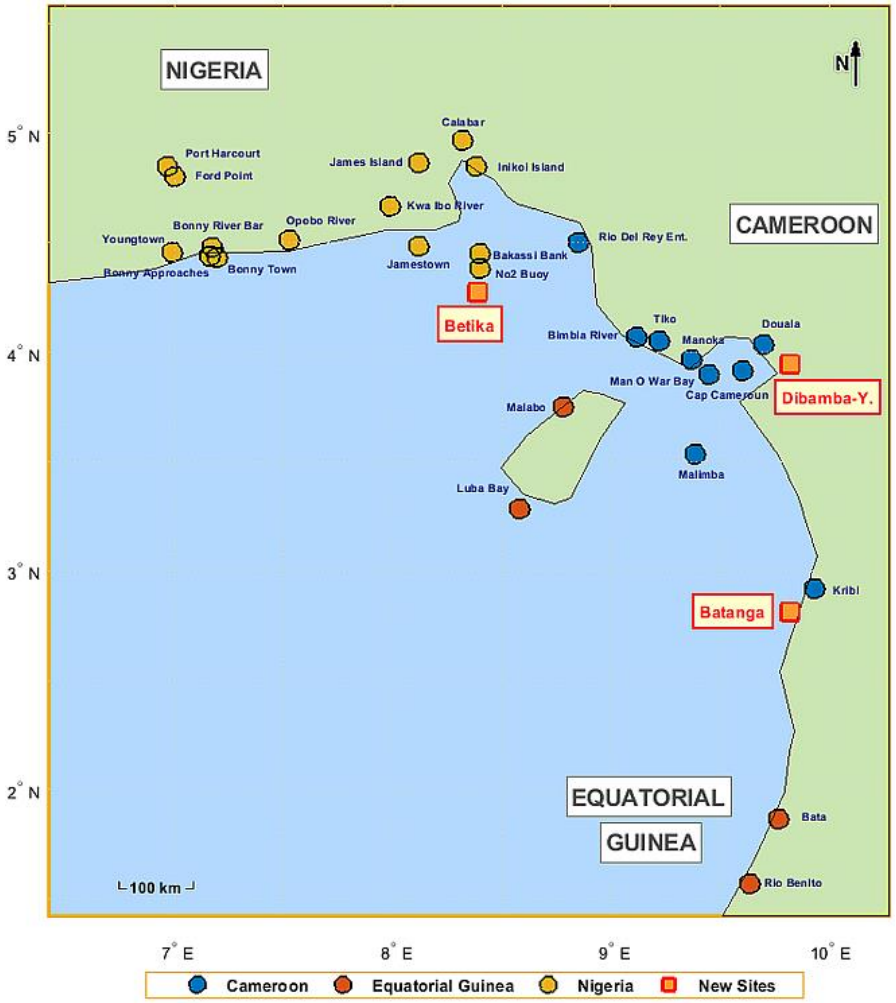

Figure 2. Location of the three test sites Betika, Dibamba-Yassa, and Batanga used for MSL-LAT offset interpolation in the Gulf of Guinea.

Table 2. Location of Selected Test Sites (WGS84 Coordinates).

Parameter	Dibamba-Yassa	Betika	Batanga
Geographic Coord. (WGS84)	Lat=03°56'26" N Lon=009°49'14" E	Lat=04°16'27" N Lon=008°23'07" E	Lat=02°48'48" N Lon=009°49'00" E
Water Depth (LAT)	5.0 m	21.5 m	30.0 m

2.4. Problem Formulation

The fundamental problem addressed in this study is that of geostatistical prediction. Let $z(s_i)$ denote the MSL-LAT value at spatial location s_i, and let $\{(s_i, z_i)\}_{i=1}^{n}$ represent the set of n reference gauged ports with known observations. The objective is to estimate z(s_0) at ungauged site s_0 given {(si, zi)} at n reference ports. Distances use the Haversine[4] formula Eq. (2) [31, 32]; the neighbourhood selects nearest stations within a prescribed radius, with k_{opt} determined by LOO cross-validation [33, 34].

$$d = 2R\arcsin\left(\sqrt{\sin^2\left(\frac{\Delta\phi}{2}\right) + \cos(\phi_1)\cos(\phi_2)\sin^2\left(\frac{\Delta\lambda}{2}\right)}\right) \quad (2)$$

where R≈6371 km, ϕ_1 and ϕ_2 are geodetic latitudes, and Δϕ, Δλ are latitude/longitude differences in radians.

Six interpolation methods are evaluated, each embodying distinct assumptions about the spatial structure of the phenomenon.

2.4.1. Nearest Neighbour (NN)

A non-parametric, deterministic algorithm based exclusively on the geometric proximity criterion with distance minimisation. At any unmeasured point x_0, the observed value Z at the closest control point x_k is assigned:

$$\hat{Z}(x_0) = Z(x_k) \text{ with } k = \arg\min_i d(x_0, x_i) \quad (3)$$

where $d(x_0, x_i)$ is the geodetic distance.

2.4.2. Inverse-distance Weighting (IDW)

The IDW estimator, following the classical Shepard formulation computes the value at x_0 as [35]:

$$\hat{Z}(x_0) = \frac{\sum_{i=1}^{n} w_i Z(x_i)}{\sum_{i=1}^{n} w_i} \quad (4)$$

with wi=1/d(x0,xi)^p and p=2 (default). The algorithm includes an adaptive optimisation of the parameter p based on leave-one-out cross-validation, and numerical stabilisation is achieved by adding ε = 10^{-6} to avoid division by zero.$w_i = \frac{1}{d(x_0,x_i)^p} p$. To better accommodate directional variability in coastal processes and the irregular clustering of reference stations, optional anisotropic and declustering corrections were incorporated.

2.4.3. Triangulation with Barycentric Interpolation (TIN)

The TIN method interpolates at point P inside a triangle (P_1, P_2, P_3) using a barycentric combination of vertex values. The estimator is written:

$$\hat{Z}(P) = \sum_{i=1}^{3} \alpha_i Z(P_i) \quad (5)$$

with closure constraint:

$$\sum_{i=1}^{3} \alpha_i = 1, \alpha_i \geq 0 \quad (6)$$

Coefficients α_i are barycentric coordinates of P with respect to the triangle, proportional to areas of opposite sub-triangles. Triangulation uses the Delaunay criterion with the Bowyer-Watson algorithm [36, 37]. Geographic coordinates are projected into the UTM system before applying barycentric interpolation to preserve local metric properties and ensure a valid Delaunay triangulation. For points outside the convex hull, an IDW fallback is applied.

2.4.4. Thin Plate Spline (TPS)

The method employs a smoothing thin-plate spline, which minimises an energy functional balancing data fidelity and surface curvature [38]:

$$J(f) = \sum_{i=1}^{n} [z_i - f(s_i)]^2 + \lambda \int \| D^2 f \|_F^2 \, dx \quad (7)$$

where si ∈Ω⊂R^2 are sample locations, zi are observations, D^2f denotes the Hessian matrix of f, and λ≥0 is the smoothing parameter controlling the trade-off between smoothing and accuracy.$s_i \in \Omega \subset \mathbb{R}^2 z_i \lambda \geq 0$.

The two-dimensional solution combines radial basis functions and a trend polynomial:

[4] The spherical approximation introduces a maximum error of ~0.5% relative to the WGS84 ellipsoid [32], which is negligible compared to the interpolation uncertainties (σ_i ≈ 2–2.5 m) of this study

$$f(x) = \sum_{j=1}^{n} a_j \ \varphi(\| x - s_j \|) + \sum_{k=1}^{m} b_k \, p_k(x) \quad (8)$$

where φ(r)=r²log(r) is the thin-plate spline kernel, and pk(x) are monomials of degree ≤1. The optimal λ is determined by generalised cross-validation (GCV) [38, 39]. $\varphi(r) = r^2 \log r \mathbb{R}^2 p_k(x) \lambda$

$$\mathrm{GCV}(\lambda) = \frac{\|\hat{z} - z\|^2}{\left(1 - \frac{\mathrm{tr}(H(\lambda))}{n}\right)^2} \quad (9)$$

where z are observed values and $\hat{z}$ = H(λ)z are fitted values via the hat matrix H(λ). TPS coefficients a and $b$are obtained by solving the augmented linear system:

$$\begin{bmatrix} K + \lambda I & P \\ P^{\top} & 0 \end{bmatrix} \begin{bmatrix} a \\ b \end{bmatrix} = \begin{bmatrix} z \\ 0 \end{bmatrix} \quad (10)$$

with Kij=φ(// s_i-s_j //), P the n×3 polynomial basis matrix (columns: 1, x, y), a∈R^n radial weights, and b∈R ³polynomial coefficients. Coordinates are projected to UTM prior to assembly. A hierarchical solver chain to ensure robustnessis used:

1) Truncated SVD (TSVD): remove singular values below $N \cdot \varepsilon_{\text{machine}} \cdot \sigma_{\max}$.
2) Calibrated Tikhonov regularisation: set $\lambda_{\text{Tik}} = \sigma_{\max}/10^4$to bound the effective condition number to $\leq 10^8$.

If all remedies fail, the procedure falls back to inverse distance weighting (IDW). In SVD coordinates the Tikhonov filter factor for singular component i is:

$$f_i = \frac{\sigma_i}{\sigma_i^2 + \lambda^2}, \quad (11)$$

which smoothly attenuates unstable modes rather than truncating them.

2.4.5. Trend Surface Analysis

This method models the MSL-LAT field as an explicit polynomial function of spatial coordinates. For a polynomial order q, the estimated surface is expressed as:

$$\hat{Z}(x, y) = \sum_{i+j \leq q} \beta_{ij} \, x^i y^j \quad (12)$$

where x, y are the planimetric coordinates. Coefficients β_{ij} are estimated by ordinary least-squares regression, with adaptive neighbour selection based on local station density:

$$\hat{\beta} = (X^T X)^{-1} X^T Z \quad (13)$$

Neighbour selection follows an adaptive criterion:

$$N_{eff} = \min\left(N_{max}, \frac{\pi R^2}{\rho}\right) \quad (14)$$

where R is the search radius (km), ρ is the mean station density (stations/km²), and N_{max} is a configurable maximum of stations (default 10). The product $\pi R^2 \rho$ yields the expected number of stations within a circular area of radius R, thus adapting the neighbourhood to the local data density.

Spatial weighting accounts for station reliability and hydrodynamic connectivity. This is incorporated into the weighted least-squares solution, where the coefficient vector $\hat{\boldsymbol{\beta}}$ is obtained by minimising:

$$\sum_{i=1}^{N_{\text{eff}}} w_i \left(Z_i - \sum_j \beta_j X_{ij}\right)^2 \quad (15)$$

leading to the standard weighted normal equations:

$$\hat{\beta} = (\mathrm{X}^{\mathrm{T}}\mathrm{W}\mathrm{X})^{-1}\mathrm{X}^{\mathrm{T}}\mathrm{W}\mathrm{Z} \quad (16)$$

with $\mathrm{W} = \mathrm{diag}(w_i)$. The weight w_i is defined as:

$$w_i = \exp\left(-\frac{d_i^2}{2\sigma_d^2}\right) \times C(\phi_i, \lambda_i) \quad (17)$$

where d_i is the Haversine distance from the estimation point to station i, and σ_d is a characteristic distance scale (e.g., half the mean inter station spacing). The factor $C(\phi_i, \lambda_i)$ enforces coastal basin connectivity and reflects shared hydrodynamic regime.

$$C = \begin{cases} 1.0 & \text{same basin (direct hydrodynamic connection)} \\ 0.5 & \text{adjacent basin (limited tidal coherence)} \\ 0.1 & \text{distant basin (no tidal coherence)} \end{cases} \quad (18)$$

2.4.6. Kriging

Ordinary Kriging first developed by Krige [40] and formalized by Matheron [20], provides the Best Linear Unbiased Estimator (BLUE) by exploiting the spatial covariance structure of the field. To estimate the value $Z(x_0)$ at an unsampled point x_0 from the known values $Z(x_i)$ at reference stations:

$$\hat{Z}(x_0) = \sum_{i=1}^{n} \lambda_i \ Z(x_i) \quad (19)$$

Weights λ_i are determined by minimising estimation variance under the unbiasedness constraint:

$$\sum_{i=1}^{n} \lambda_i = 1 \quad (20)$$

Spatial dependence is quantified by the variogram $\gamma(\mathrm{h})$, defined as the semi-variance of increments:

$$\gamma(h) = \frac{1}{2} \ \mathrm{Var}[Z(x) - Z(x + h)] \quad (21)$$

The experimental variogram is computed from n reference

stations:

$$\hat{\gamma}(h_k) = \frac{1}{2N(h_k)} \sum_{|x_i - x_j| \in [h_k - \Delta/2,\, h_k + \Delta/2]} \left[Z(x_i) - Z(x_j)\right]^2 \quad (22)$$

where h_k is the k-th distance interval (bin), $N(h_k)$ is the number of station pairs in that bin, and Δ is the bin width. The empirical variogram is fitted by one of the five following theoretical models.

Table 3. Theoretical variogram models.

Model	Variogram formula $\gamma(h)$
Spherical	$c_0 + c\left[1.5\left(\frac{h}{a}\right) - 0.5\left(\frac{h}{a}\right)^3\right], h \le a;\ \ c_0 + c, h > a$
Exponential	$c_0 + c\left[1 - \exp\left(-\frac{h}{a}\right)\right]$
Gaussian	$c_0 + c\left[1 - \exp\left(-\left(\frac{h}{a}\right)^2\right)\right]$
Matern 3/2	$c_0 + c\left[1 - \left(1 + \sqrt{3}\frac{h}{a}\right)\exp\left(-\sqrt{3}\frac{h}{a}\right)\right]$
Matern 5/2	$c_0 + c\left[1 - \left(1 + \sqrt{5}\frac{h}{a} + \frac{5h^2}{3a^2}\right)\exp\left(-\sqrt{5}\frac{h}{a}\right)\right]$

where c_0 is nugget, c is sill, a is range. Parameters are estimated by nonlinear least-squares. Optimal weights are obtained by solving the ordinary Kriging system:

$$\begin{bmatrix} \gamma_{11} & \gamma_{12} & \cdots & \gamma_{1n} & 1 \\ \gamma_{21} & \gamma_{22} & \cdots & \gamma_{2n} & 1 \\ \vdots & \vdots & \ddots & \vdots & \vdots \\ \gamma_{n1} & \gamma_{n2} & \cdots & \gamma_{nn} & 1 \\ 1 & 1 & \cdots & 1 & 0 \end{bmatrix} \begin{bmatrix} \lambda_1 \\ \lambda_2 \\ \vdots \\ \lambda_n \\ \mu \end{bmatrix} = \begin{bmatrix} \gamma_{10} \\ \gamma_{20} \\ \vdots \\ \gamma_{n0} \\ 1 \end{bmatrix} \quad (23)$$

with $\gamma_{ij} = \gamma(\| x_i - x_j \|)$ and $\gamma_{0i} = \gamma(\| x_0 - x_i \|)$. The Lagrange multiplier μ enforces the unbiasedness constraint. Numerical stability is ensured by adding a regularization nugget $\varepsilon = 10^{-10}$ to the diagonal. Persistently ill-conditioned systems are handled by a fallback chain based on TSVD, Tikhonov regularization, QR decomposition, and finally IDW. For Universal Kriging, the model includes a polynomial trend structure:

$$Z(x) = m(x) + \varepsilon(x) = \sum_{k=0}^{K} a_k\ f_k(x) + \varepsilon(x) \quad (24)$$

where $m(x)$ denotes the deterministic trend, for example a polynomial in the spatial coordinates, a_k are the associated coefficients, and $\varepsilon(x)$ is a zero-mean stationary residual. The estimator then becomes:

$$\hat{Z}(x_0) = \hat{m}(x_0) + \sum_{i=1}^{n} \lambda_i \left[Z(x_i) - \hat{m}(x)\right] \quad (25)$$

and the augmented system:

$$\begin{cases} \sum_{j=1}^{n} \lambda_j\ \gamma(x_i, x) + \sum_{k=0}^{K} \mu_k\ f_k(x_i) = \gamma(x_i, x_0) & \forall i = 1, \ldots, n \\ \sum_{j=1}^{n} \lambda_j\ f_k(x_j) = f_k(x_0) & \forall k = 0, \ldots, K \\ \sum_{j=1}^{n} \lambda_j = 1 \end{cases} \quad (26)$$

The Matern family (ν=3/2 and ν=5/2) generalizes classical variogram models and is particularly robust for quasi-collinear station configurations and smooth coastal MSL-LAT gradients.

2.5. Cross-validation and Uncertainty Decomposition

2.5.1. Systematic Comparison Methodology for Interpolation Methods

The six interpolation methods (Nearest Neighbor, IDW, TIN, Spline, Trend Surface, Ordinary Kriging) are evaluated using a standardized framework based on a common set of 115 reference stations (ATT, GLOSS, PSMSL, UHSLC/JASL). A parametric analysis is conducted by varying the number of neighbors ($k = 1$ to 10-15) and search radius.

Performance is assessed through Leave-One-Out (LOO) cross-validation, computing MAE, RMSE, R^2, and bias. Convergence analysis (error vs. k) identifies the optimal number of neighbors k_{opt}. A composite ranking (RMSE 40%, MAE 30%, $R^2$20%, uncertainty 10%) determines the best-performing method and parameters, supported by automated outputs (Tables, heatmaps, performance diagrams).

This framework jointly defines the optimal method, k_{opt}, and spatial coverage, used for final MSL-LAT estimation.

2.5.2. Leave-One-Out (LOO) Protocol

The LOO procedure temporarily removes each station i in turn and estimates its value from the k nearest remaining stations: ei = z(xi) − ẑ(-i)(xi). Neighbour count is varied from k=1 to kmax (typically 10-12) to determine kopt as the value minimising RMSE.

$$e_i = z(x_i) - \hat{z}^{(-i)}(x_i) \tag{27}$$

where z_i is the observed value and $\hat{z}_i$ the interpolated estimate from the remaining $N-1$ stations. For each iteration: (i) exclude station i, (ii) rank neighboring stations using Haversine distance, (iii) select the k closest, (iv) apply the selected interpolation method, and (v) compute the residual.

Global performance metrics (MAE, RMSE, R^2, bias) are derived after N iterations, with k_{opt} defined as the value minimizing RMSE.

2.5.3. Statistical Performance Metrics

Performance is quantified by four standardised metrics (Table 4): MAE, RMSE, R^2, and Bias, capturing absolute accuracy, sensitivity to large errors, explained variance, and systematic error respectively.R^2

Table 4. Statistical Evaluation Metrics.

Metric	Formula	Interpretation
MAE	$\frac{1}{N}\sum_{t=1}^{N}\|\|e_t\|\|$	Mean Absolute Error: mean absolute deviation between observed and estimated values.
RMSE	$\sqrt{\frac{1}{N}\sum_{t=1}^{N}e_t^2}$	Root Mean Square Error: strongly penalises large and outlying errors.
R^2	$1-\frac{\sum_{t=1}^{N}[Z(\mathbf{x}_t)-\hat{Z}_{(-t)}(\mathbf{x}_t)]^2}{\sum_{t=1}^{N}[Z(\mathbf{x}_t)-\hat{Z}]^2}$	Coefficient of Determination: proportion of variance explained (Z=mean of observations).
Bias	$\frac{1}{N}\sum_{t=1}^{N}e_t$	Systematic Bias: tendency to consistently under- or over-estimate values.

2.5.4. Convergence Analysis

k_{opt} was selected via a plateau-detection algorithm (3-point moving average; first k with relative improvement <2% over three increments). This prevents overfitting to noisy minima; a clear MAE minimum was used when no plateau existed. Performance classification used R^2 and RMSE thresholds: EXCELLENT for $R^2 \geq 0.80$, RMSE<0.10 m, GOOD for $R^2 \geq 0.50$, RMSE<0.15 m, ACCEPTable: $R^2 \geq 0.10$, RMSE<0.30 m, LIMITED: $R^2 < 0.10$ or RMSE≥0.30 m. A weighted composite score based on normalized RMSE, MAE, R^2, and confidence interval ranked the methods.

$$\text{Score} = 0.40\ \text{RMSE}_n + 0.30\ \text{MAE}_n + 0.20\ R_n^2 + 0.10\ \text{CI}_n \tag{28}$$

Components were normalized to across methods; the highest score determined the preferred method.

2.5.5. Total Uncertainty Model

Following the ISO-GUM framework for measurement uncertainty, total variance is decomposed as [13]:

$$\sigma_t^2 = \sigma_i^2 + \sigma_d^2 + \sigma_m^2 \tag{29}$$

where σ_i reflects spatial configuration and density (from LOO-CV), σ_d reflects source data uncertainty, and σ_m reflects inter-method variability. The 95% confidence interval for the prediction at location s_0 is[5]:

$$CI_{95} = \hat{z}(s_0) \pm 1.960\ \sigma_{\text{total}} \tag{30}$$

2.6. LSUHydroTide Software Implementation

2.6.1. Software Components

All six interpolation methods are implemented in the LSUHydroTide (Java/Swing) application via a centralized PortInterpolation class. Each method integrates advanced features, including LOO-CV-based parameter optimisation, anisotropy handling, variogram fitting, and numerical fallback chains

[5] The 1.960 factor assumes the normal approximation. For small samples, the 95% interval is based on the Student-t distribution

(TSVD → Tikhonov → IDW) for ill-conditioned systems, and automated composite scoring. LOO-CV, performance evaluation (MAE, RMSE, R^2, bias), convergence analysis, and uncertainty decomposition (σ_t) are fully automated. Method selection relies on a composite score (RMSE 40%, MAE 30%, $R^2$20%, uncertainty 10%), aligned with IHO S-44 thresholds. Numerical stability is ensured through regularization, nugget constraints, and TSVD-based solvers. The system produces standardized, reproducible validation PDF reports.

2.6.2. Analytical Visualisations

The software generates scatter plots, convergence curves, performance bar charts, and inter-method correlation heatmaps within a multi-tab interface, together with a synthetic decision report including method rankings and operational recommendations.

3. Results and Analysis

Results are presented for three sites in contrasted configurations. For each: (i) reference network, (ii) comparative method performance, (iii) optimal method analysis, (iv) uncertainty decomposition, (v) adopted MSL-LAT offset. Performance classification follows IHO S-44 thresholds (Section 2.5.4).

3.1. Betika (Rio Del Rey Shelf): Moderate Network with Inter-method Discrimination

3.1.1. Reference Network Characteristics

Betika (4°16′N, 8°23′E) is on the Rio del Rey shelf in a Cameroon-Nigeria-Equatorial Guinea transboundary context. The network includes 18 stations within 133 km. Nine stations were retained for the final cross-validation after convergence analysis. Inter-station distances range from 12.2 to 133.0 km (mean=78.3 km), with spatial extent of 1.73° lat × 2.25° lon, density of 0.347 stations/1,000 km², and a noTable outlier at Calabar (MSL-LAT=2.09 m at 77.4 km) that tests algorithm robustness with respect to extreme values (Table 5).

3.1.2. Comparative Performance of the Six Methods

Table 6 presents the comparative performances of the six methods evaluated by leave-one-out cross-validation on 18 stations (k_{max}=12). Figure 4 visually summarises results in a comparative Table generated by LSUHydroTide with colour-coding (gold: 1st rank, silver: 2nd, bronze: 3rd).

No	Port Name	Country	Latitude	Longitude	MSL-LAT (m)	Distance (km)
1	No 2 Buoy (Calabar River)	Nigeria	04° 22' 60" N	08° 24' 00" E	1.10	12.2
2	Bakassi Bank (Calabar River)	Nigeria	04° 27' 00" N	08° 24' 00" E	1.22	19.6
3	Jamestown (Calabar River)	Nigeria	04° 28' 60" N	08° 07' 01" E	1.48	37.8
4	Rio Del Rey Entrance	Cameroon	04° 30' 00" N	08° 50' 60" E	1.41	57.3
5	Kwa Ibo River Entrance	Nigeria	04° 39' 58" N	07° 59' 18" E	1.13	61.9
6	Inikoi Island (Akpa Yafe River)	Nigeria	04° 50' 60" N	08° 22' 60" E	1.60	64.0
7	James Island (Calabar River)	Nigeria	04° 52' 00" N	08° 07' 01" E	1.34	72.3
8	Malabo	Equatorial Guinea	03° 45' 00" N	08° 46' 60" E	1.16	73.1
9	Calabar (Calabar River)	Nigeria	04° 58' 00" N	08° 19' 01" E	2.09	77.4
10	Jamestown	Nigeria	05° 01' 00" N	08° 22' 60" E	1.48	82.6
11	Entrance - Bimbia River	Cameroon	04° 04' 00" N	09° 07' 01" E	1.10	84.4
12	Port Sonara (Limbé) (GLOSS)	Cameroon	04° 00' 18" N	09° 07' 30" E	1.20	87.3
13	Tiko - Bimbia River	Cameroon	04° 02' 60" N	09° 13' 01" E	1.20	95.5
14	Opobo River Entrance (Sandy ...	Nigeria	04° 30' 53" N	07° 31' 42" E	1.10	98.7
15	Bahia de Luba (San Carlos)	Equatorial Guinea	03° 16' 60" N	08° 34' 60" E	1.02	112.3
16	Man O War Bay	Cameroon	03° 58' 00" N	09° 22' 01" E	1.20	114.1
17	Cap Cameroun	Cameroon	03° 53' 60" N	09° 26' 60" E	1.40	125.2
18	Bonny River Bar	Nigeria	04° 25' 47" N	07° 11' 44" E	1.43	133.0

Figure 3. *Spatial distribution of the 18 reference stations around Betika (colour-coded by distance: green <30 km, yellow 30-70 km, red >70 km). Source: LSUHydroTide.*

Table 5. Reference Network Parameters for the Betika Site.

Parameter	Value
Available stations (100 km radius)	18
Retained stations (CV	9
Inter-station distances (km)	12.2 - 133.0 (mean ≈ 78.3)
Spatial extent (lat × lon)	≈ 1.73° × 2.25°
Spatial variance σ² (m²)	0.0611 (σ ≈ 0.25 m; CV=18.8%)
Station density / 1,000 km²	0.347
Mean MSL-LAT of 18 stations (m)	1.31
MSL-LAT range (m)	1.02 (Bahia de Luba) - 2.09 (Calabar)

IDW clearly dominates (RMSE=0.2295 m, R^2=0.1376, global score=0.370) and is the only method to display a significantly positive R^2, indicating real capacity to capture the spatial structure. Kriging ranks second (RMSE=0.2343 m, R^2=0.1007) also with a slightly positive R^2. Both are classified "AccepTable" according to the IHO S-44 scale.

Figures 5-7 present scatter plots, convergence curves, and a comparative performance chart for Betika.

Table 6. Comparative Performance of Interpolation Methods for Betika (leave-one-out, 18 stations, kmax=12).

Rank	Method	Score	σ_t (m)	Level
1	IDW	0.370	±2.479	AccepTable
2	Kriging	0.358	±2.479	AccepTable
3	TIN	0.219	±2.483	Limited
4	Trend	0.069	±2.488	Limited
5	NN	-0.125	±2.493	Limited
6	Spline	-0.149	±2.494	Limited

Average RMSE	Average R²	Best Method	Performance Gap
0.2917 m	-0.4357	Inverse Distance ...	55.2%

Rank	Method	MAE (m)	RMSE (m)	R²	Bias (m)	Optimal k	Uncertainty (m)	Performance
1	Inverse Distance Weighting...	0.1748	0.2295	0.1376	0.0120	9	0.2703	Poor
2	Kriging	0.1698	0.2343	0.1007	0.0100	6	0.2962	Poor
3	Triangulation (TIN)	0.2105	0.2706	-0.1990	-0.0038	6	0.2748	Poor
4	Trend Surface	0.2264	0.3095	-0.5687	-0.0173	2	0.4594	Poor
5	Nearest Neighbor	0.2850	0.3501	-1.0069	-0.0628	1	0.3906	Poor
6	Spline	0.2808	0.3562	-1.0777	-0.0036	3	0.4188	Poor

Figure 4. Comparative performance Table of the six interpolation methods for Betika (LOO cross-validation, kmax=12). Source: LSUHydroTide.

Kriging ranks second, with the spherical variogram well-constrained over 18 stations. TIN ranks third (RMSE=0.2706 m), while Trend Surface, NN, and Spline show Limited performance (RMSE 0.31-0.36 m), confirming their unsuitability at this scale.

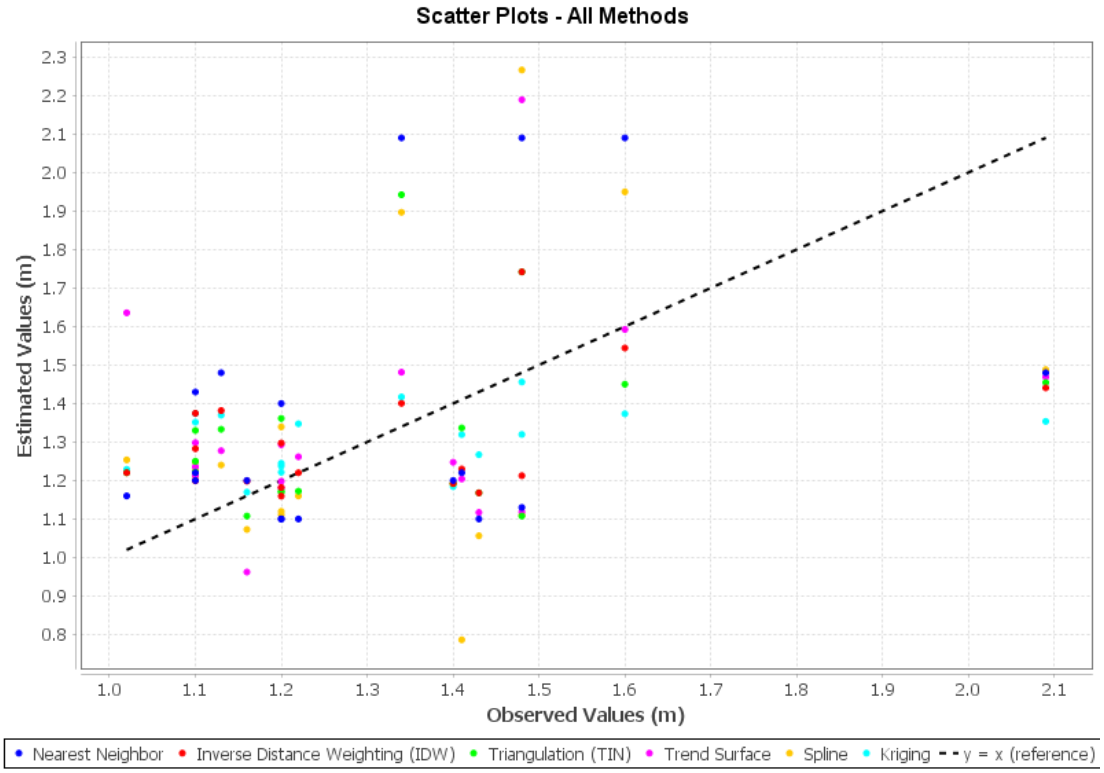

Figure 5. Multi-method scatter plot for Betika (Observed vs. Estimated). Each colour represents a method; the dashed black line=perfect prediction y=x. Source: LSUHydroTide.

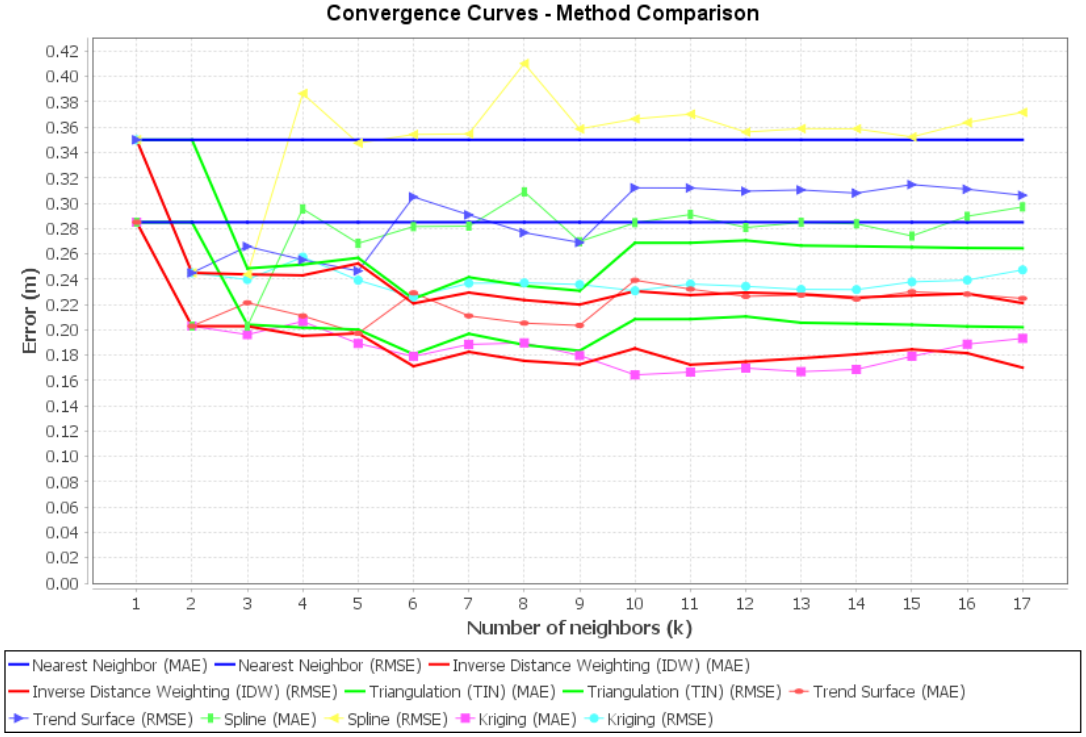

Figure 6. MAE and RMSE convergence curves as a function of the number of neighbours k for the six methods at Betika. Solid lines=MAE, dashed lines=RMSE. Source: LSUHydroTide.

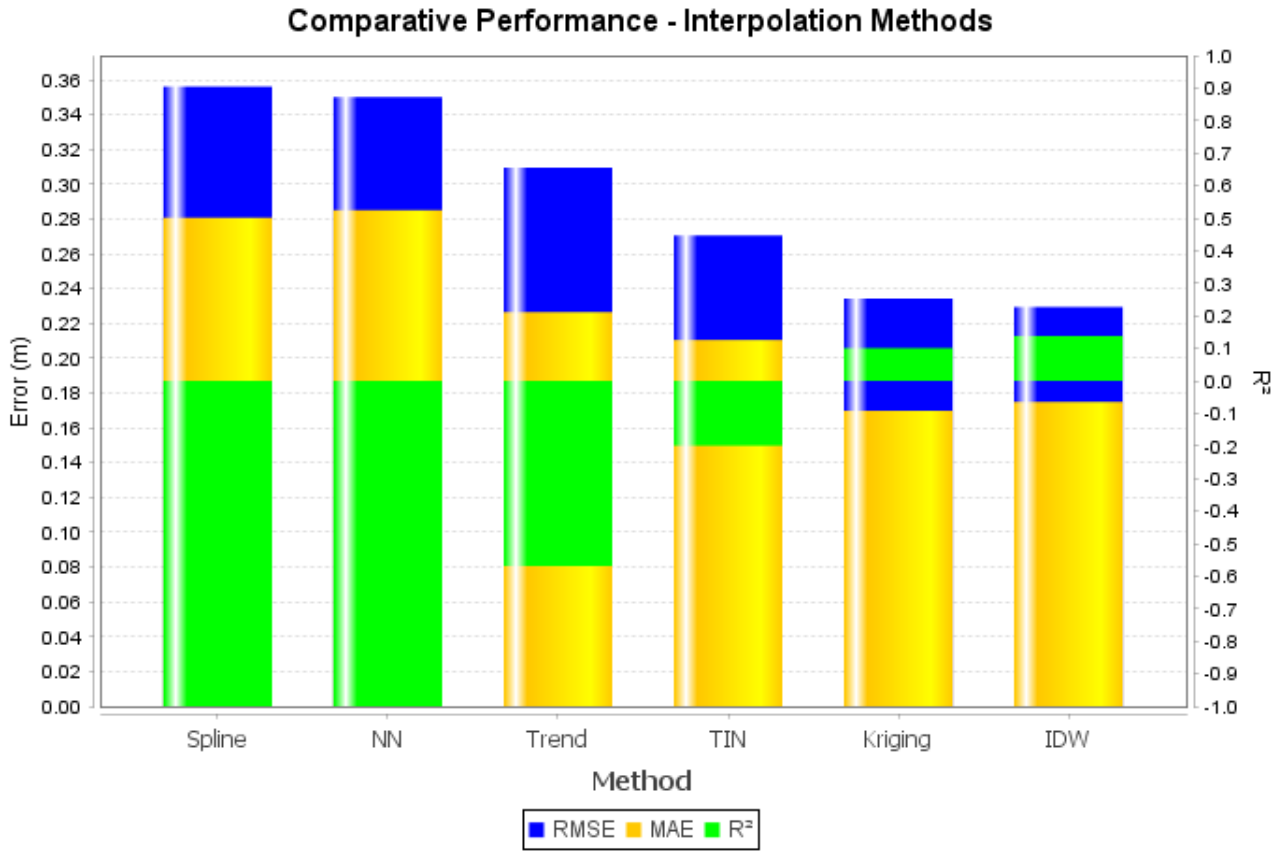

Figure 7. Comparative performance chart of the six interpolation methods at Betika (RMSE in blue, MAE in orange, R² in green on secondary axis). Source: LSUHydroTide.

3.1.3. Inter-method Correlations

The correlation matrix (Table 7, Figure 8) shows high cross-correlations among NN, IDW, and Spline (r=0.89-0.92), moderate IDW-Kriging correlation (r=0.785), and lower TIN-Trend values. The broad 18-station coverage avoids strong anti-correlation blocks, reflecting distributed predictive information across all methods.

Table 7. Inter-Method Correlation Matrix for Betika Site.

Method	NN	IDW	TIN	Trend	Spline	Kriging
NN	1.000	0.893	0.896	0.722	0.923	0.712
IDW	0.893	1.000	0.768	0.837	0.890	0.785
TIN	0.896	0.768	1.000	0.692	0.815	0.721
Trend	0.722	0.837	0.692	1.000	0.845	0.597
Spline	0.923	0.890	0.815	0.845	1.000	0.640
Kriging	0.712	0.785	0.721	0.597	0.640	1.000

Method	Nearest Neighbor	Inverse Distance ...	Triangulation (TIN)	Trend Surface	Spline	Kriging
NN	1.000	0.893	0.896	0.722	0.923	0.712
IDW	0.893	1.000	0.768	0.837	0.890	0.785
TIN	0.896	0.768	1.000	0.692	0.815	0.721
Trend	0.722	0.837	0.692	1.000	0.845	0.597
Spline	0.923	0.890	0.815	0.845	1.000	0.640
Kriging	0.712	0.785	0.721	0.597	0.640	1.000

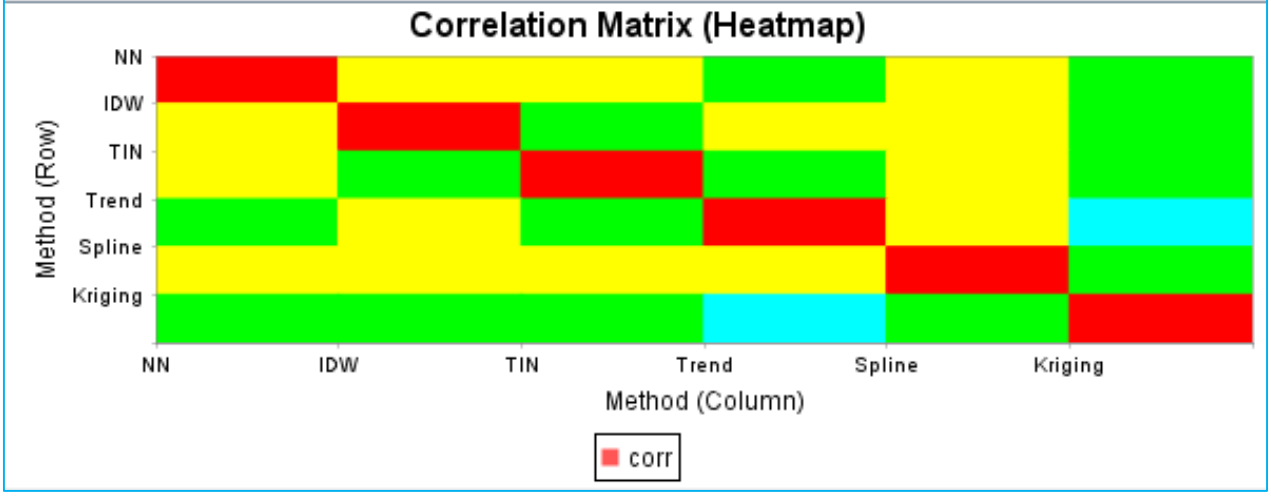

Figure 8. *Inter-method correlation matrix heatmap at Betika (red=strong, yellow=weak/negative). Source: LSUHydroTide.*

3.1.4. IDW Cross-validation and Uncertainty Decomposition

IDW with k_{opt}=9 is retained. Figures 9-14 show retained stations, evaluation metrics, scatter plot, convergence curve, uncertainty decomposition, and station performance.

No	Port Name	Country	Latitude	Longitude	MSL-LAT (m)	Distance (km)
1	No 2 Buoy (Calabar River)	Nigeria	04° 22' 60" N	08° 24' 00" E	1.10	12.2
2	Bakassi Bank (Calabar River)	Nigeria	04° 27' 00" N	08° 24' 00" E	1.22	19.6
3	Jamestown (Calabar River)	Nigeria	04° 28' 60" N	08° 07' 01" E	1.48	37.8
4	Rio Del Rey Entrance	Cameroon	04° 30' 00" N	08° 50' 60" E	1.41	57.3
5	Kwa Ibo River Entrance	Nigeria	04° 39' 58" N	07° 59' 18" E	1.13	61.9
6	Inikoi Island (Akpa Yafe River)	Nigeria	04° 50' 60" N	08° 22' 60" E	1.60	64.0
7	James Island (Calabar River)	Nigeria	04° 52' 00" N	08° 07' 01" E	1.34	72.3
8	Malabo	Equatorial Guinea	03° 45' 00" N	08° 46' 60" E	1.16	73.1
9	Calabar (Calabar River)	Nigeria	04° 58' 00" N	08° 19' 01" E	2.09	77.4
10	Jamestown	Nigeria	05° 01' 00" N	08° 22' 60" E	1.48	82.6
11	Entrance - Bimbia River	Cameroon	04° 04' 00" N	09° 07' 01" E	1.10	84.4

Figure 9. *Stations retained for IDW leave-one-out cross-validation at Betika (18-station LOO network, kopt=9). Source: LSUHydroTide.*

Metric	Value	Interpretation
MAE (Mean Absolute Error)	0.235 m	Good
RMSE (Root Mean Square Error)	0.278 m	Good
R^2 (Coefficient of Determination)	0.021	Low
Systematic Bias	-0.037 m	Negligible
Recommended k (LOO convergence)	9	Statistically optimal number of neighbors
User selected k	1	Manual GUI selection

Figure 10. *IDW cross-validation evaluation metrics at Betika: MAE=0.1748 m, RMSE=0.2295 m, R^2=0.1376, bias=+0.012 m, kopt=9. Source: LSUHydroTide.*

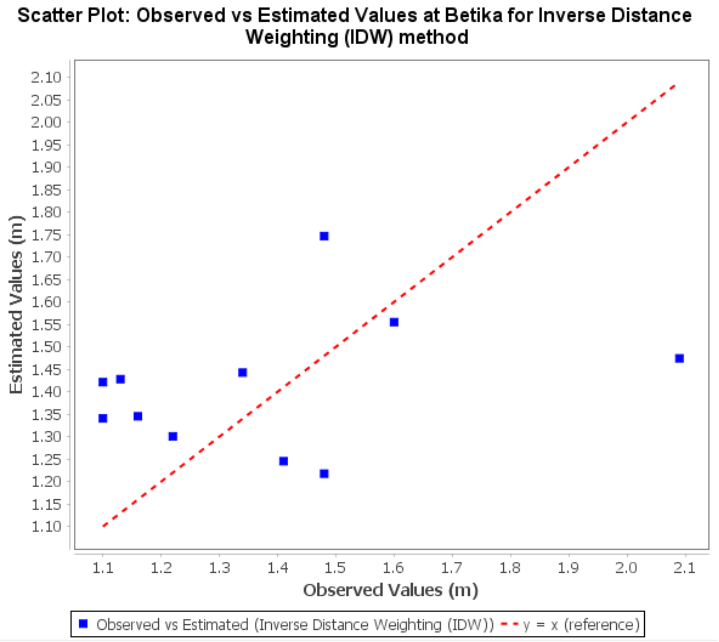

Figure 11. *Observed vs. Estimated scatter plot for the IDW method in cross-validation at Betika. The red dashed line represents perfect prediction y=x. Source: LSUHydroTide.*

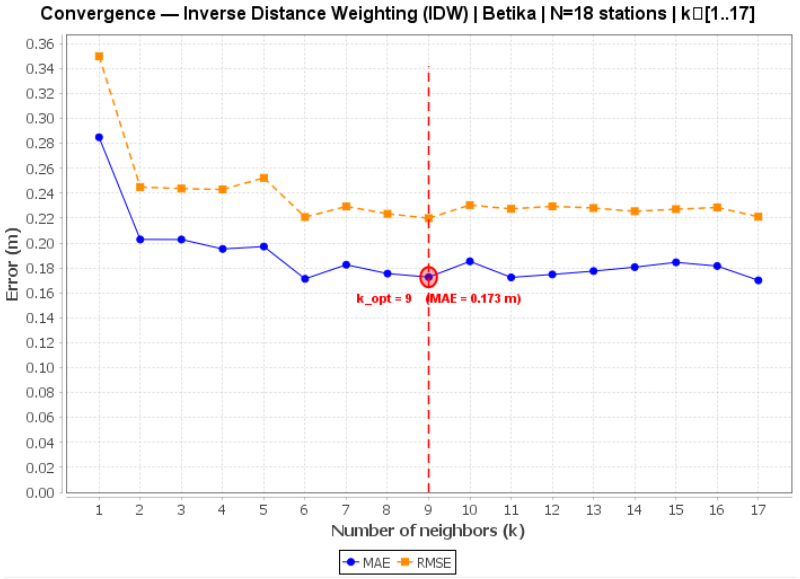

Figure 12. *MAE and RMSE convergence curve as a function of k for the IDW method at Betika. The red point marks kopt=9. Source: LSUHydroTide.*

The scatter plot (Figure 11) shows concentration around y=x in [1.10-1.60 m], with slight dispersion at extremes (Inikoi Island 1.60 m, Calabar 2.09 m), consistent with IDW's distance-weighting mechanism. The estimated MSL-LAT offset is concentrated in the interval [1.20 m - 1.50 m].

The IDW convergence curve (Figure 12) shows monotonic error decrease to k=9, then a plateau, confirming k_{opt}=9 as the optimal neighbourhood size.

The uncertainty budget (Figure 13, Table 8) shows $\sigma_i^2 \approx$ 6.08 m² (≈96% of total), identical across all methods. σ_d^2 ranges from 0.053 m² (IDW) to 0.123 m² (NN), while σ_m^2 = 0.010 m² is constant, confirming that algorithm choice is marginal.

The most problematic stations are Kwa Ibo River Entrance (26.4% error) and Entrance-Bimbia River (29.2%), reflecting local MSL-LAT anomalies not captured by broader spatial interpolation (Figure 14).

Table 8. *Uncertainty Budget Decomposition for Betika (Retained IDW Method).*

Component	Value (m²)	Share in σ_t^2 (%)
σ_i^2 (interpolation variance, spatial configure)	6.0827	≈ 96%
σd² (data source quality -IDW)	0.0527	≈ 1%
σd² (data source quality -NN)	0.1225	(reference)
σm² (model specification -all methods)	0.0098	< 1%
σ_t (IDW)	±2.479 m	-
CI_{95} (IDW)	±4.859 m	-

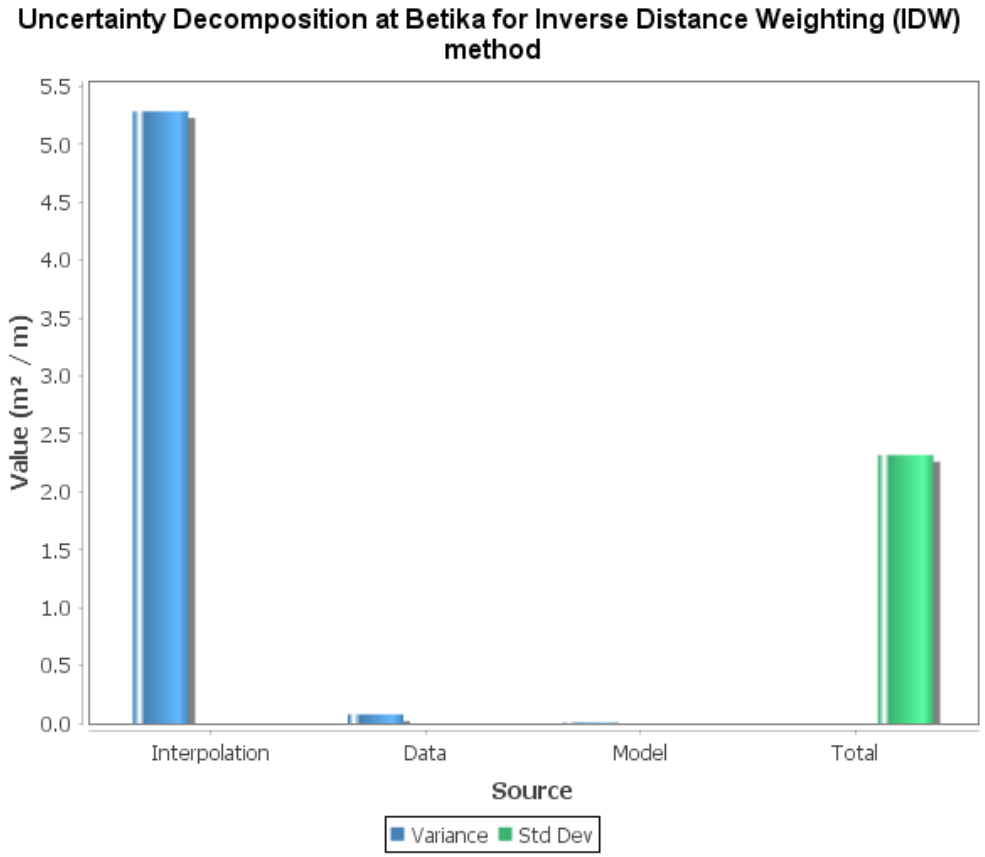

Figure 13. *Uncertainty source decomposition for the IDW method in cross-validation at Betika. The dominance of σ_i^2 (spatial configuration) is overwhelming. Source: LSUHydroTide.*

Station	Observed (m)	Estimated (m)	Error (m)	Abs Error (%)
No 2 Buoy (Calabar River)	1.100	1.341	-0.241	21.87%
Bakassi Bank (Calabar River)	1.220	1.301	-0.081	6.61%
Jamestown (Calabar River)	1.480	1.218	0.262	17.72%
Rio Del Rey Entrance	1.410	1.245	0.165	11.68%
Kwa Ibo River Entrance	1.130	1.428	-0.298	26.39%
Inikoi Island (Akpa Yafe River)	1.600	1.555	0.045	2.80%
James Island (Calabar River)	1.340	1.443	-0.103	7.66%
Malabo	1.160	1.345	-0.185	15.97%
Calabar (Calabar River)	2.090	1.474	0.616	29.46%
Jamestown	1.480	1.747	-0.267	18.03%
Entrance - Bimbia River	1.100	1.422	-0.322	29.23%

Figure 14. *Station-by-station performance for the IDW method at Betika (error <15 cm=green, 15-30 cm=yellow, >30 cm=red). Source: LSUHydroTide.*

3.1.5. Offset and Operational Reliability

The IDW method with k_{opt}=9 produces an interpolated MSL-LAT offset of 1.147 m for Betika (Figure 15), with a bias of +0.012 m.

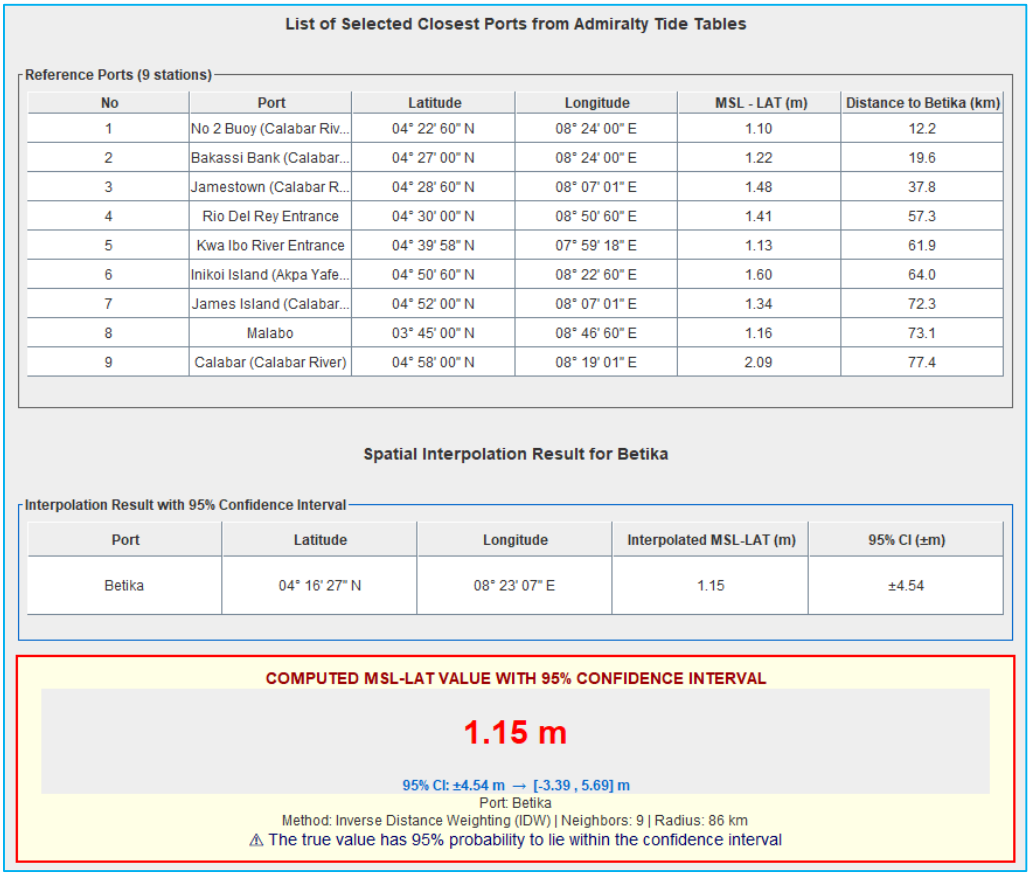

Figure 15. *Spatial interpolation result (IDW method, kopt=9) for the Betika site: estimated MSL-LAT offset=1.147 m. Source: LSUHydroTide.*

Performance ranges from moderate to accepTable; the 95% CI of ±4.859 m requires conservative vertical margins. Network densification to the south (2-3 additional stations at 65-133 km) is the priority improvement.

3.2. Dibamba-Yassa (Wouri Estuary): Locally Coherent Network, High Regional Uncertainty

3.2.1. Reference Network Characteristics

Dibamba-Yassa (Lat=03°56′26″N, Lon=09°49′14″E) lies in the turbid Wouri Estuary with semi-diurnal mesotidal regime. Six stations are available within 65.8 km, mostly to the west. Spatial variance (σ^2=0.0209 m²; CV=10.6%) indicates a relatively homogeneous MSL-LAT field, though Douala (1.62 m, 16.9 km) introduces a noTable high value (Table 9).

Table 9. Reference Network Parameters for Dibamba-Yassa Site.

Parameter	Value
Available stations (68 km radius)	6
Minimum inter-station distance (km)	11.8
Maximum inter-station distance (km)	65.8
Mean inter-station distance (km)	37.0
Spatial extent (lat × lon)	≈ 0.52° × 0.48°
Spatial variance σ^2 (m²)	0.0209 ($\sigma \approx 0.145$ m; CV=10.6%)
Station density / 1,000 km²	1.766
Mean MSL-LAT of 6 stations (m)	1.36
MSL-LAT range (m)	1.20 (Tiko-Bimbia River) - 1.62 (Douala)

3.2.2. Comparative Performance of the Six Methods

Table 10 and Figure 17 present the comparative performances. In contrast to Betika, the Trend Surface method dominates with a clearly positive R^2 (R^2=0.2833, RMSE=0.1225 m, score=0.539), reaching "Good" performance level. Kriging ranks second (RMSE=0.1439 m) and NN third (RMSE=0.1454 m). TIN is also AccepTable (0.1571 m), while Spline and IDW show Limited performance with negative R^2.

No	Port Name	Country	Latitude	Longitude	MSL-LAT (m)	Distance (km)
1	Douala	Cameroon	04° 01' 60" N	09° 41' 60" E	1.62	16.9
2	Manoka	Cameroon	03° 55' 00" N	09° 35' 60" E	1.42	24.6
3	Cap Cameroun	Cameroon	03° 53' 60" N	09° 26' 60" E	1.40	41.4
4	Man O War Bay	Cameroon	03° 58' 00" N	09° 22' 01" E	1.20	50.4
5	Malimba	Cameroon	03° 31' 60" N	09° 22' 60" E	1.32	66.4
6	Tiko - Bimbia River	Cameroon	04° 02' 60" N	09° 13' 01" E	1.20	68.0

Figure 16. Spatial distribution of the 6 reference stations around Dibamba-Yassa (colour-coded by distance). Source: LSUHydroTide.

Average RMSE	Average R^2	Best Method	Performance Gap
0.1535 m	-0.1432	Trend Surface	45.1%

Rank	Method	MAE (m)	RMSE (m)	R^2	Bias (m)	Optimal k	Uncertainty (m)	Performance
1	Trend Surface	0.0965	0.1225	0.2833	0.0028	4	0.1527	Poor
2	Kriging	0.1139	0.1439	0.0110	0.0092	2	0.1703	Poor
3	Nearest Neighbor	0.1167	0.1454	-0.0096	0.0233	1	0.3217	Poor
4	Triangulation (TIN)	0.1369	0.1571	-0.1797	0.0013	3	0.1817	Poor
5	Spline	0.1578	0.1746	-0.4555	0.0536	2	0.1969	Poor
6	Inverse Distance Weighting...	0.1613	0.1777	-0.5090	-0.0046	2	0.1997	Poor

Figure 17. Comparative pesrformance Table of the six interpolation methods for Dibamba-Yassa (leave-one-out cross-validation, kmax=12). Source: LSUHydroTide.

Multi-method scatter plot (Figure 18) confirms these results visually: Trend Surface points remain closest to the y = x line across the observed range [1.20-1.62 m].

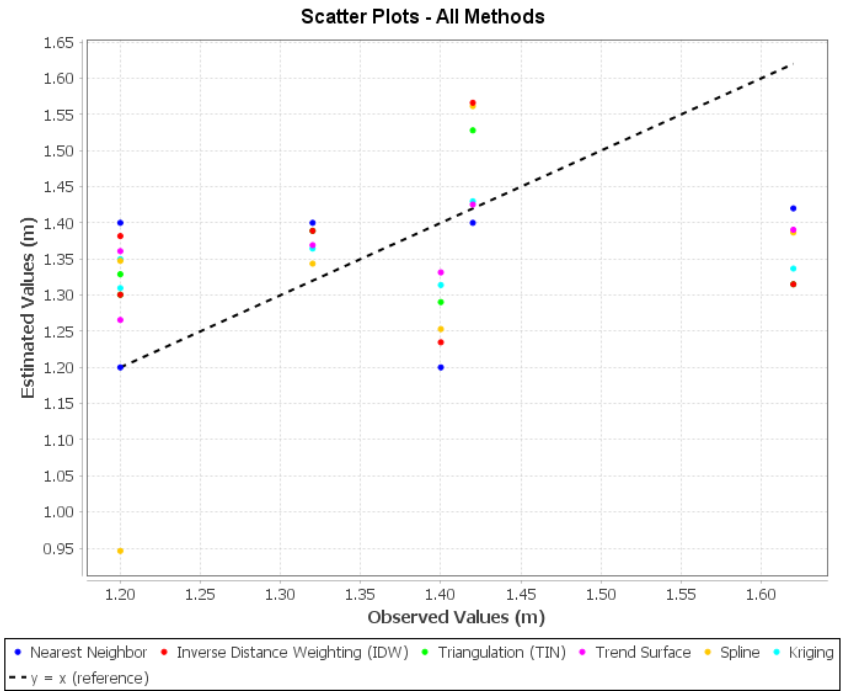

Figure 18. *Multi-method scatter plot for Dibamba-Yassa (Observed vs. Estimated). The tendency to underestimate for Douala (1.62 m) is visible for most methods. Source: LSUHydroTide.*

Convergence curves (Figure 19) show Trend Surface reaching k_{opt}=4 early, while IDW degrades monotonically with k. Trend Surface's early stabilisation reflects the polynomial surface adapting well to the spatially coherent estuary field despite few stations. Kriging converges rapidly (k_{opt} = 2), effectively capturing covariance structure using only the two closest stations (Douala, Manoka).

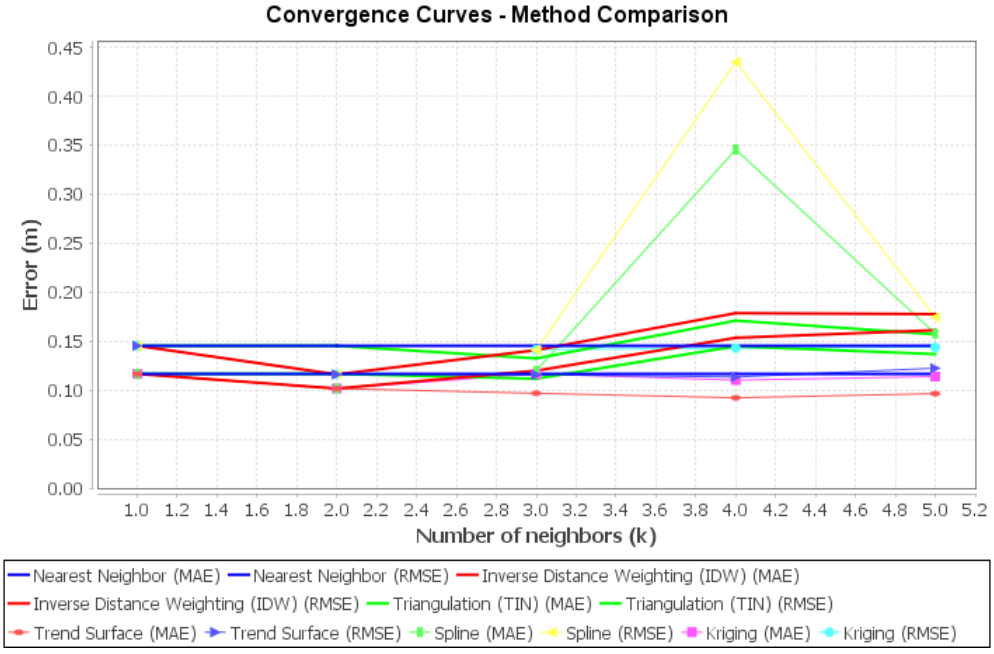

Figure 19. *MAE and RMSE convergence curves as a function of k for the six methods at Dibamba-Yassa. Rapid Kriging convergence (kopt=2) and Trend Surface optimum at kopt =4 are noteworthy. Source: LSUHydroTide.*

Table 10. Comparative Performance of Interpolation Methods for Dibamba-Yassa (leave-one-out, 6 stations, kmax=12).

Rank	Method	Score	σ_t (m)	Level
1	Trend	0.539	±2.117	Good
2	Kriging	0.431	±2.118	AccepTable
3	NN	0.423	±2.119	AccepTable
4	TIN	0.352	±2.119	AccepTable
5	Spline	0.245	±2.121	Limited
6	IDW	0.224	±2.121	Limited

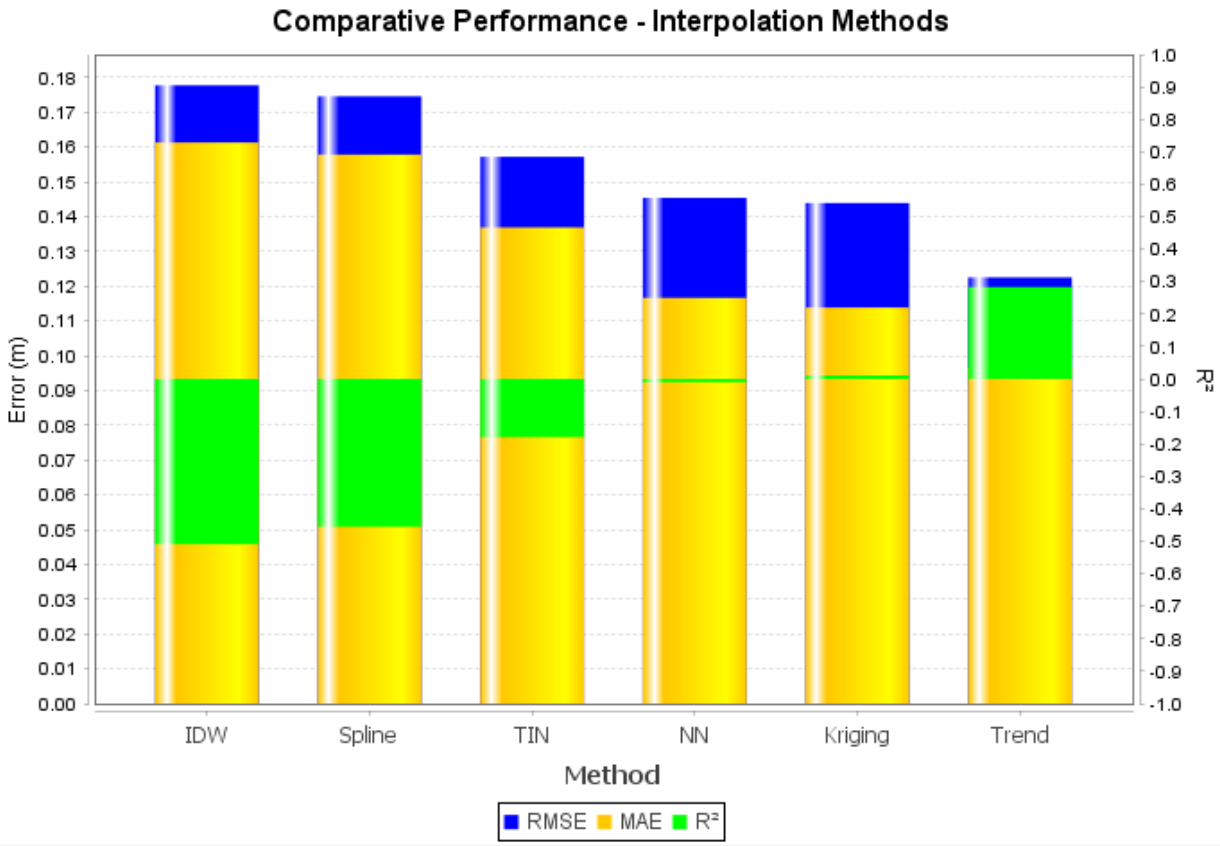

Figure 20. Comparative performance chart at Dibamba-Yassa (RMSE, MAE, R²). The tight hierarchy reflects low spatial variability of the MSL-LAT field in the estuary. Source: LSUHydroTide.

Performance comparison chart (Figure 20) illustrates the method hierarchy at Dibamba-Yassa: Trend Surface clearly leads with the lowest error bars and highest R². Kriging and NN are competitive at the "AccepTable" level, while IDW and Spline are limited.

3.2.3. Inter-method Correlations

Table 11. Inter-Method Correlation Matrix for Dibamba-Yassa Site.

Method	NN	IDW	TIN	Trend	Spline	Kriging
NN	1.000	0.624	0.512	0.830	0.780	0.654

Method	NN	IDW	TIN	Trend	Spline	Kriging
IDW	0.624	1.000	0.959	0.695	0.681	0.972
TIN	0.512	0.959	1.000	0.709	0.701	0.978
Trend	0.830	0.695	0.709	1.000	0.988	0.813
Spline	0.780	0.681	0.701	0.988	1.000	0.810
Kriging	0.654	0.972	0.978	0.813	0.810	1.000

The correlation matrix (Table 11, Figure 21) shows two clusters: IDW, TIN, and Kriging are tightly correlated (r=0.96-0.98), while Trend Surface and Spline form a separate cluster (r=0.99). NN shows moderate cross-cluster correlations (r=0.51-0.83), reflecting fundamentally different prediction surfaces from polynomial vs. distance-based methods.

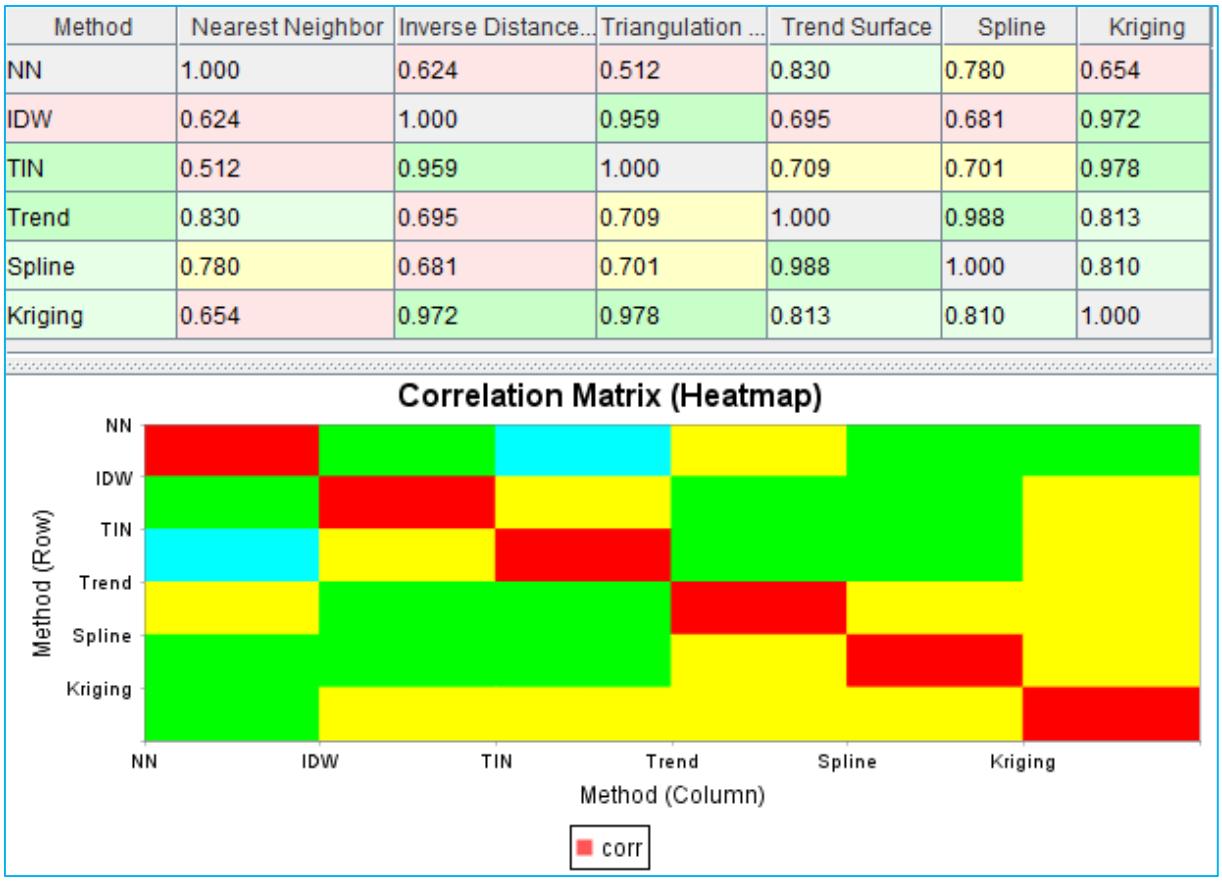

Figure 21. *Inter-method correlation matrix heatmap at Dibamba-Yassa. Source: LSUHydroTide.*

3.2.4. Trend Surface Cross-validation and Uncertainty Decomposition

The Trend Surface method with k_{opt}=4 neighbours (56 km radius, 4 stations) is retained for the final estimation. Figures 22-27 present the selected stations, dedicated cross-validation metrics, scatter plot, convergence curve, uncertainty decomposition, and station-by-station performance.

Reference Ports for Interpolation

Method: Trend Surface | Target Port: Dibamba-Yassa | k = 4

No	Port Name	Country	Latitude	Longitude	MSL-LAT (m)	Distance (km)
1	Douala	Cameroon	04° 01' 60" N	09° 41' 60" E	1.62	16.9
2	Manoka	Cameroon	03° 55' 00" N	09° 35' 60" E	1.42	24.6
3	Cap Cameroun	Cameroon	03° 53' 60" N	09° 26' 60" E	1.40	41.4
4	Man O War Bay	Cameroon	03° 58' 00" N	09° 22' 01" E	1.20	50.4

Figure 22. *Stations retained for Trend Surface leave-one-out cross-validation at Dibamba-Yassa (4 stations, 56 km radius). Source: LSUHydroTide.*

Metric	Value	Interpretation
MAE (Mean Absolute Error)	0.135 m	Good
RMSE (Root Mean Square Error)	0.152 m	Good
R^2 (Coefficient of Determination)	-0.040	Low
Systematic Bias	0.011 m	Negligible
Recommended k (LOO convergence)	4	Statistically optimal number of neighbors
User selected k	1	Manual GUI selection

Figure 23. *Trend Surface dedicated cross-validation evaluation metrics at Dibamba-Yassa (4-station sub-network, kopt=4): MAE=0.1354 m, RMSE=0.1516 m, R^2=-0.040, bias=+0.011 m.*

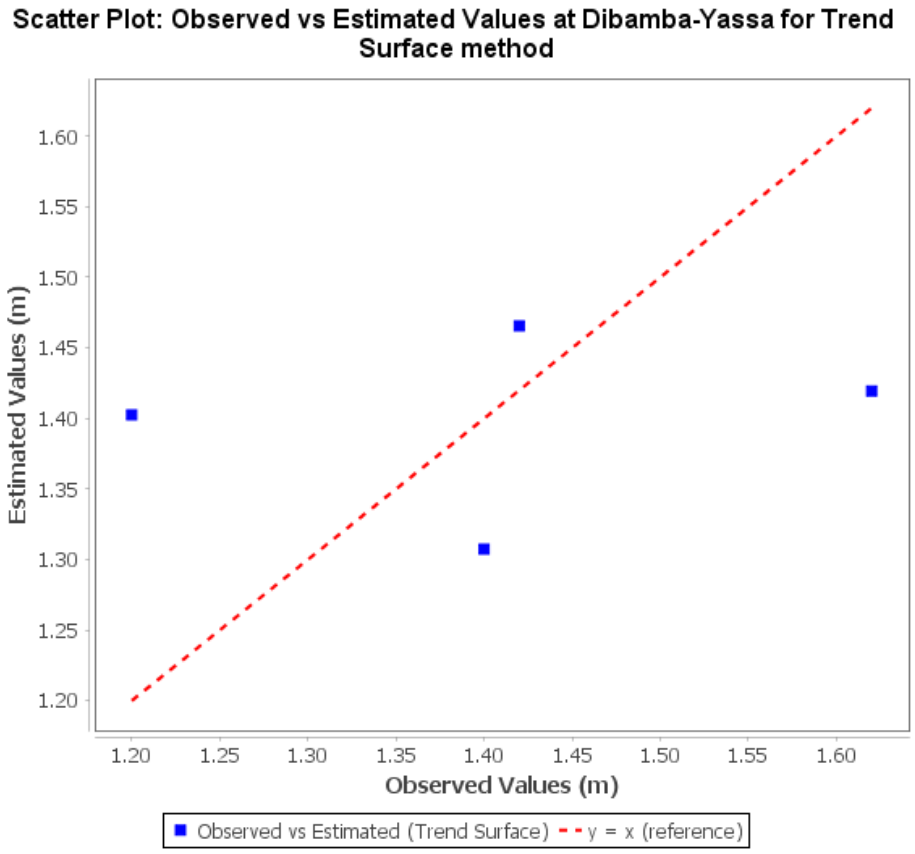

Figure 24. *Observed vs. Estimated scatter plot for Trend Surface cross-validation at Dibamba-Yassa. Source: LSUHydroTide.*

Station	Observed (m)	Estimated (m)	Error (m)	Abs Error (%)
Douala	1.620	1.419	0.201	12.38%
Manoka	1.420	1.466	-0.046	3.22%
Cap Cameroun	1.400	1.307	0.093	6.61%
Man O War Bay	1.200	1.403	-0.203	16.88%

Figure 25. *Station-by-station performance for Trend Surface at Dibamba-Yassa. Douala and Man O War Bay concentrate most residual error. Source: LSUHydroTide.*

The scatter plot (Figure 24) reveals a generally good fit: Douala (1.62 m, est. 1.419 m; error 12.4%) and Man O War Bay (1.20 m, est. 1.403 m; error 16.9%) carry the largest residuals, while Manoka (3.2%) and Cap Cameroun (6.6%) are well estimated (Figure 25). The polynomial trend surface nonetheless effectively captures the general spatial gradient across the estuary, explaining its superior R^2 compared to distance-weighted methods.

The convergence curve (Figure 26) confirms Trend Surface stabilisation at k=4, with the polynomial coefficients best constrained by all 4 available stations. The MAE at k_{opt} = 0.1354 m demonstrates the method's accuracy in this spatially coherent environment.

Uncertainty decomposition (Figure 27 and Table 12) shows σ_i^2=4.461 m² (>95%). σ_d^2=0.015 m² for Trend Surface is the lowest among methods, confirming its data efficiency. CI_{95}=±4.149 m (6 stations) reduces to ±3.595 m for the dedicated 4-station validation.

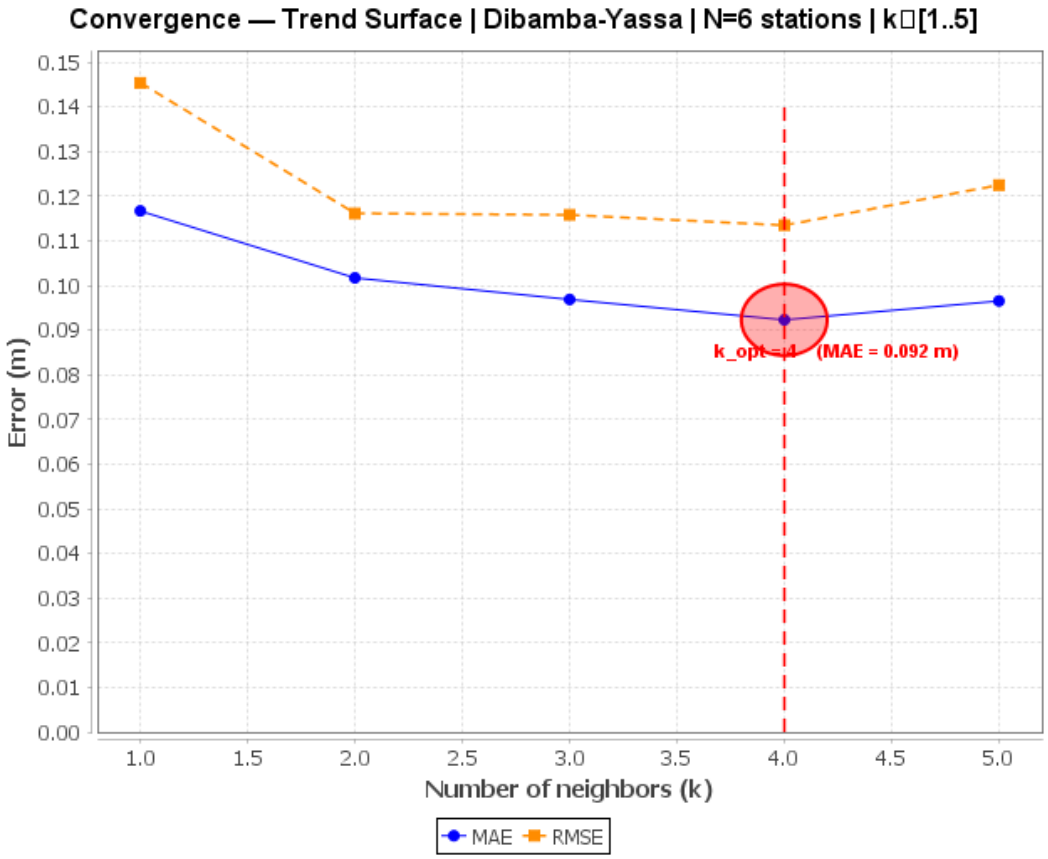

Figure 26. *MAE and RMSE convergence curve for Trend Surface at Dibamba-Yassa. Stabilisation from k=4 (kopt, red point). Source: LSUHydroTide.*

Table 12. Uncertainty Budget Decomposition for Dibamba-Yassa (Retained Trend Surface Method).

Component	Value (m²)	Share in σ_t^2 (%)
σ_i^2 (interpolation variance, spatial configure)	4.4610	> 95%
σd^2 (data quality - Trend Surface)	0.0150	≈ 1%
σd^2 (data quality - NN)	0.0211	(reference)
σm^2 (model specification - all methods)	0.0058	< 1%
σ_t (Trend Surface, 6 stations)	±2.117 m	-
CI_{95} (Trend Surface, 6 stations)	±4.149 m	-
σ_t (Trend Surface, dedicated validation - 4 stations)	±1.834 m	-
CI_{95} (Trend Surface, dedicated validation)	±3.595 m	-

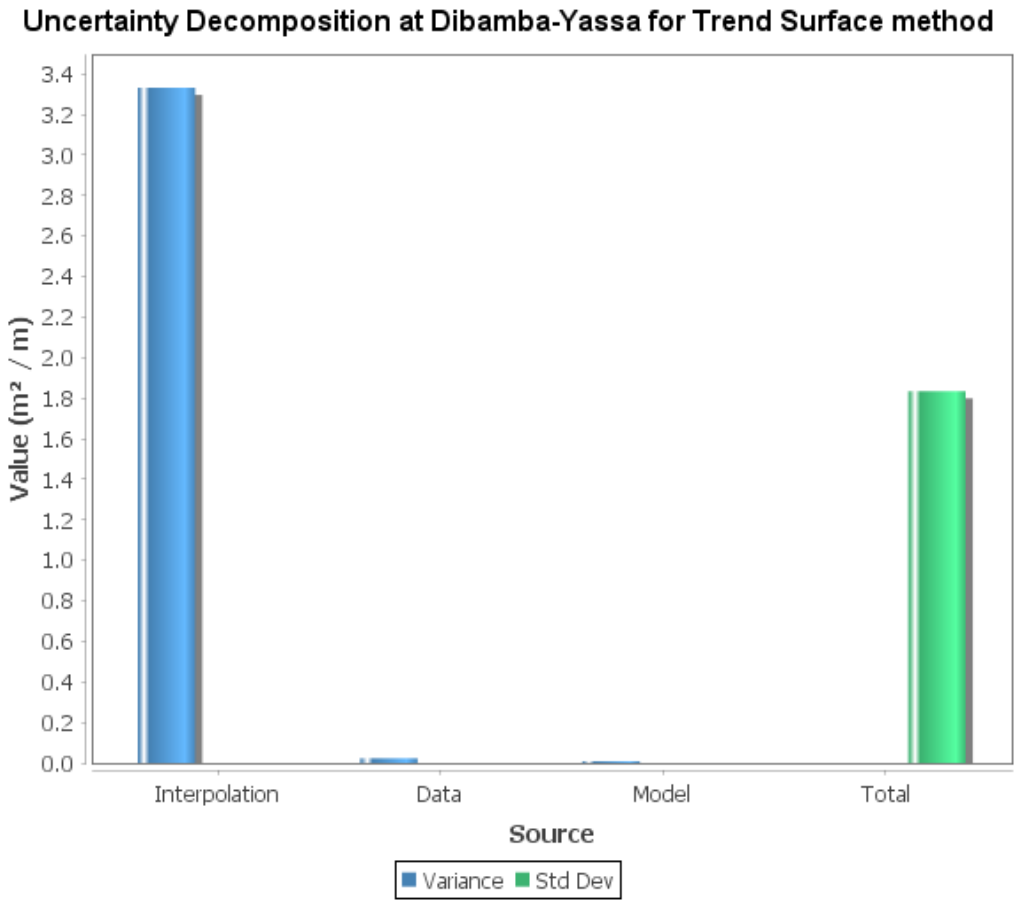

Figure 27. Uncertainty source decomposition for Trend Surface at Dibamba-Yassa. σ_i^2 dominance is systematic. Source: LSUHydroTide.

3.2.5. MSL-LAT Offset and Operational Reliability

Trend Surface with k_{opt}=4 produces an MSL-LAT offset of 1.571 m for Dibamba-Yassa (Figure 28), with bias of +0.011 m.

Performance level is Good (R^2=0.2833) despite only 4 stations. The polynomial trend effectively captures the spatial gradient across the estuary. However, CI_{95}=±3.595 m means in-situ validation by temporary tide gauge is recommended for critical applications.

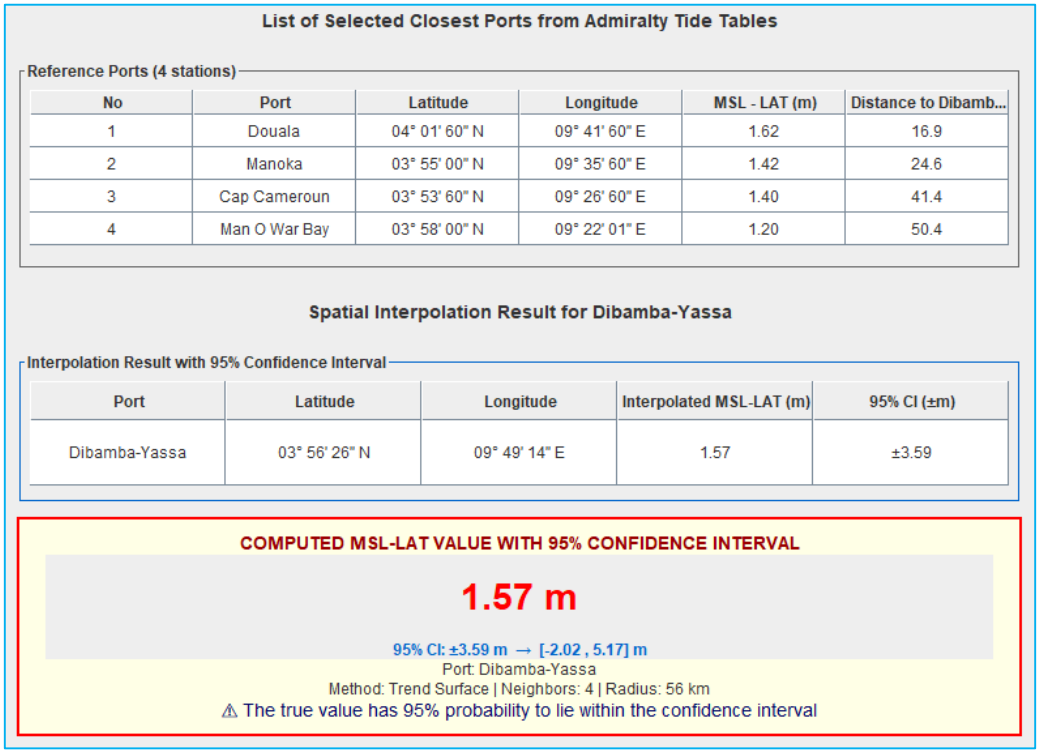

List of Selected Closest Ports from Admiralty Tide Tables

Reference Ports (4 stations)

No	Port	Latitude	Longitude	MSL - LAT (m)	Distance to Dibamb...
1	Douala	04° 01' 60" N	09° 41' 60" E	1.62	16.9
2	Manoka	03° 55' 00" N	09° 35' 60" E	1.42	24.6
3	Cap Cameroun	03° 53' 60" N	09° 26' 60" E	1.40	41.4
4	Man O War Bay	03° 58' 00" N	09° 22' 01" E	1.20	50.4

Spatial Interpolation Result for Dibamba-Yassa

Interpolation Result with 95% Confidence Interval

Port	Latitude	Longitude	Interpolated MSL-LAT (m)	95% CI (±m)
Dibamba-Yassa	03° 56' 26" N	09° 49' 14" E	1.57	±3.59

COMPUTED MSL-LAT VALUE WITH 95% CONFIDENCE INTERVAL

1.57 m

95% CI: ±3.59 m → [-2.02 , 5.17] m
Port: Dibamba-Yassa
Method: Trend Surface | Neighbors: 4 | Radius: 56 km
⚠ The true value has 95% probability to lie within the confidence interval

Figure 28. *Spatial interpolation result (Trend Surface method, kopt=4) for Dibamba-Yassa: estimated MSL-LAT offset=1.571 m. Source: LSUHydroTide.*

3.3. Batanga (Southern Cameroon): Problem Degeneration Through Extreme Undersampling

3.3.1. Reference Network Characteristics

No	Port Name	Country	Latitude	Longitude	MSL-LAT (m)	Distance (km)
1	Kribi	Cameroon	02° 55' 00" N	09° 55' 60" E	1.00	17.3
2	Malimba	Cameroon	03° 31' 60" N	09° 22' 60" E	1.32	93.4

Figure 29. *Spatial distribution of the 2 reference stations around Batanga. Total absence of stations in all directions except north-south illustrates the extreme undersampling. Source: LSUHydroTide.*

Table 13. *Reference Network Parameters for Batanga Site.*

Parameter	Value
Number of available stations	2 (Kribi and Malimba)
Distances to site (km)	17.3 (Kribi, south); 93.4 (Malimba, north)
Mean distance to site (km)	55.4
Spatial extent (lat × lon)	≈ 0.62° × 0.55°
MSL-LAT of stations (m)	1.00 (Kribi); 1.32 (Malimba)
Spatial variance σ^2 (m^2)	≈ 0.0256 (n=2, statistically non-significant)
Station density / 1,000 km^2	≈ 0.302
Coefficient of variation CV (%)	13.8 (uninterpreTable with n=2)

Batanga lies on a poorly instrumented open coast. Only two stations bracket the site (Figure 29): Kribi (MSL-LAT=1.00 m, 17.3 km south) and Malimba (1.32 m, 93.4 km north, Table 13). Spatial variance ($\sigma^2 \approx 0.0256$ m²) is non-significant with n=2.

The density of 0.30 stations/1,000 km² and the mean distance of 55.4 km from the site place Batanga in the category of insufficient networks according to all criteria of the convergence analysis.

3.3.2. Method Performance and Degeneration Analysis

With only two points, all methods reduce to a linear combination of the two values, yielding strictly identical metrics (RMSE=0.320 m; R^2=−3.00; score=−0.716). The scatter plot (Figure 31), performance chart (Figure 32), and correlation heatmap (Figure 33) all visually confirm this mathematical degeneration.

Table 14. *Comparative Performance of Methods for Batanga Site (Total Degeneration).*

Rank	Method	Score	σ_t (m)	Level
1-6	All methods	-0.716	±2.375	Unusable

Average RMSE	Average R^2	Best Method	Performance Gap
0.3200 m	NaN	Nearest Neighbor	0.0%

Rank	Method	MAE (m)	RMSE (m)	R^2	Bias (m)	Optimal k	Uncertainty (m)	Performance
1	Nearest Neighbor	0.3200	0.3200	NaN	0.0000	1	0.3262	Poor
2	Inverse Distance Weightin...	0.3200	0.3200	NaN	0.0000	1	0.3262	Poor
3	Triangulation (TIN)	0.3200	0.3200	NaN	0.0000	1	0.3262	Poor
4	Trend Surface	0.3200	0.3200	NaN	0.0000	1	0.3262	Poor
5	Spline	0.3200	0.3200	NaN	0.0000	1	0.3262	Poor
6	Kriging	0.3200	0.3200	NaN	0.0000	1	0.3262	Poor

Figure 30. *Comparative method Table at Batanga. Perfect identity of metrics for all methods illustrates the mathematical degeneration of the interpolation problem with n=2 stations. Source: LSUHydroTide.*

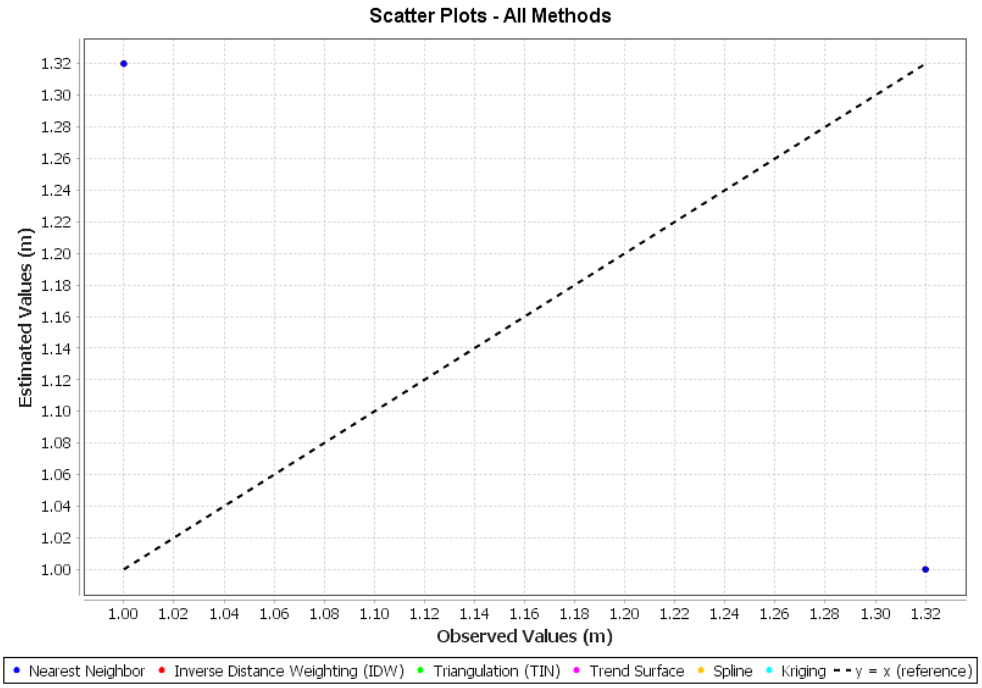

Figure 31. *Multi-method scatter plot at Batanga. Perfect superposition of all points and symmetry with respect to y=x illustrate the problem degeneration. Source: LSUHydroTide.*

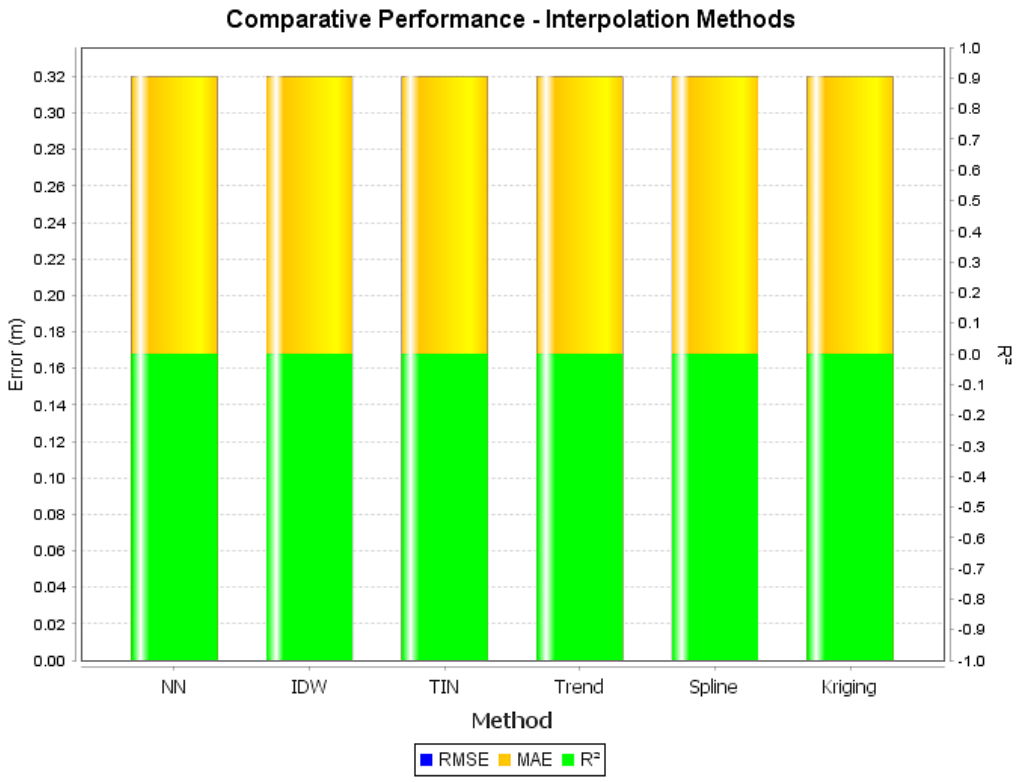

Figure 32. Comparative performance chart at Batanga. Strict identity of RMSE and MAE bars for all methods is the visual signal of degeneration. Source: LSUHydroTide.

Method	Nearest Neighb...	Inverse Distance...	Triangulation ...	Trend Surface	Spline	Kriging
NN	1.000	1.000	1.000	1.000	1.000	1.000
IDW	1.000	1.000	1.000	1.000	1.000	1.000
TIN	1.000	1.000	1.000	1.000	1.000	1.000
Trend	1.000	1.000	1.000	1.000	1.000	1.000
Spline	1.000	1.000	1.000	1.000	1.000	1.000
Kriging	1.000	1.000	1.000	1.000	1.000	1.000

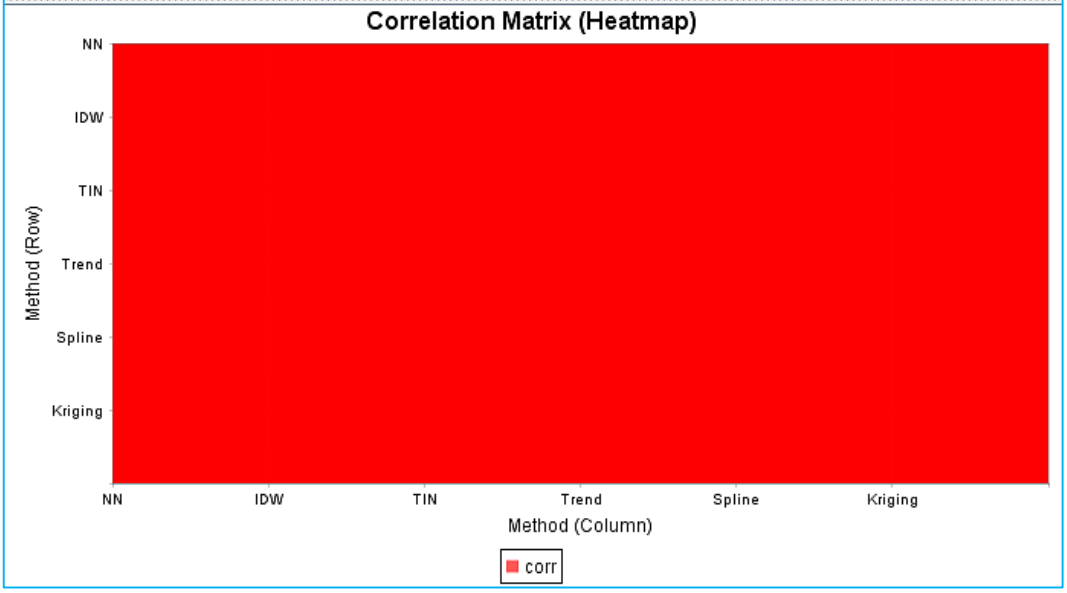

Figure 33. Inter-method correlation matrix heatmap at Batanga. High correlations confirm near-identity of predictions under undersampling. Source: LSUHydroTide.

(Figure 33) shows very high correlations between most methods (r > 0.9 for IDW, Spline, Kriging, and NN), confirming near-identity of their predictions.

3.3.3. Cross-validation and Uncertainty Decomposition

Leave-one-out cross-validation using Nearest Neighbor (Figures 34-35), selected by default as the simplest and most transparent method in this degenerate context, confirms the identical metrics observed in the global comparison.

The scatter plot (Figure 36) reduces to two perfectly symmetric points relative to y = x, while uncertainty decomposition (Figure 37, Table 15) reveals extreme estimation fragility: $\sigma_i^2 \approx 5.58$ m² accounts for >98% of total variance. The 95% CI of ±4.662 m matches the full MSL-LAT range across the Gulf of Guinea (0.50 m at St. Helena to 3.95 m at Porto Gole), rendering the estimate operationally meaningless.

Station-by-station performance (Figure 38) confirms symmetric absolute errors: 32.0% at Kribi and 24.2% at Malimba.

Reference Ports for Interpolation

Method: Nearest Neighbor | Target Port: Batanga | k = 2

No	Port Name	Country	Latitude	Longitude	MSL-LAT (m)	Distance (km)
1	Kribi	Cameroon	02° 55' 00" N	09° 55' 60" E	1.00	17.3
2	Malimba	Cameroon	03° 31' 60" N	09° 22' 60" E	1.32	93.4

Figure 34. *Stations retained for NN cross-validation at Batanga (the 2 only available). Source: LSUHydroTide.*

Metric	Value	Interpretation
MAE (Mean Absolute Error)	0.320 m	Acceptable
RMSE (Root Mean Square Error)	0.320 m	Good
R² (Coefficient of Determination)	-3.000	Low
Systematic Bias	0.000 m	Negligible
Optimal k (convergence)	1	Recommended number of neighbors

Figure 35. *NN evaluation metrics at Batanga: MAE=RMSE=0.320 m, R²=-3.000, bias=0.000 m. Source: LSUHydroTide.*

Table 15. *Uncertainty Budget Decomposition for Batanga (All Methods Combined).*

Component	Value (m²)	Share in σ_t^2 (%)
σ_i^2 (interpolation variance)	5.5826	> 98%
σd^2 (data source quality -NN)	0.1447	≈ 2%
σm^2 (model specification)	0.0032	< 0.1%
σ_t	±2.375 m	-
CI_{95}	±4.662 m	-

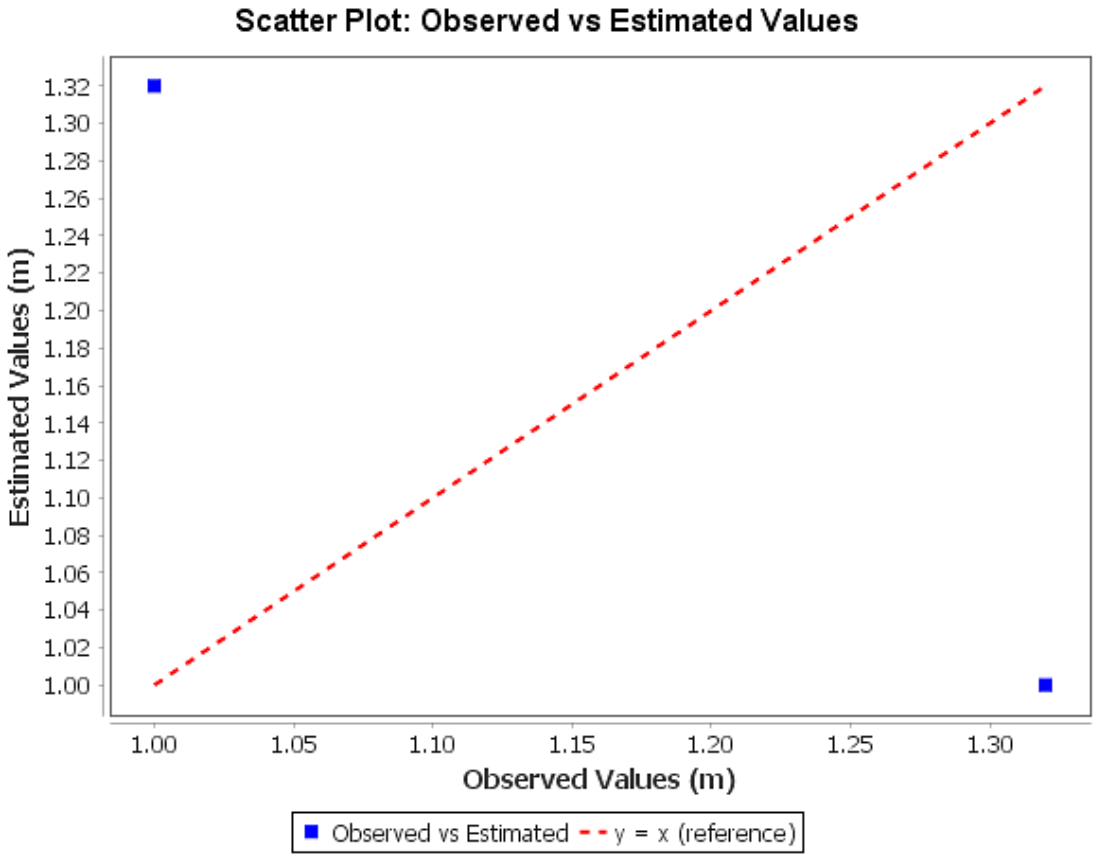

Figure 36. *NN scatter plot in cross-validation at Batanga: two symmetric points, no interpolative information. Source: LSUHydroTide.*

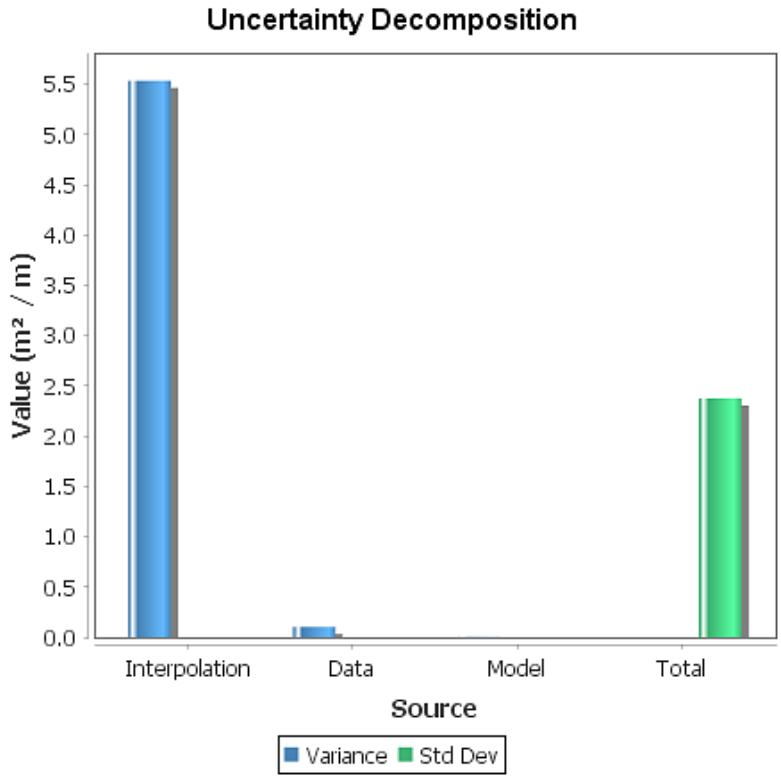

Figure 37. *Uncertainty decomposition at Batanga. Near-total dominance of σ_i^2 (>98%) shows the problem is entirely governed by network geometry. Source: LSUHydroTide.*

Station	Observed (m)	Estimated (m)	Error (m)	Abs Error (%)
Kribi	1.000	1.320	0.320	32.00%
Malimba	1.320	1.000	-0.320	24.24%

Figure 38. *Station-by-station performance for NN at Batanga. The two errors (32% and 24%) reflect only the gap between the two available values. Source: LSUHydroTide.*

3.3.4. MSL-LAT Offset and Operational Reliability

The NN method is retained by default (Figure 39), providing an MSL-LAT offset of 1.00 m (value from Kribi, the nearest station at 17.3 km).

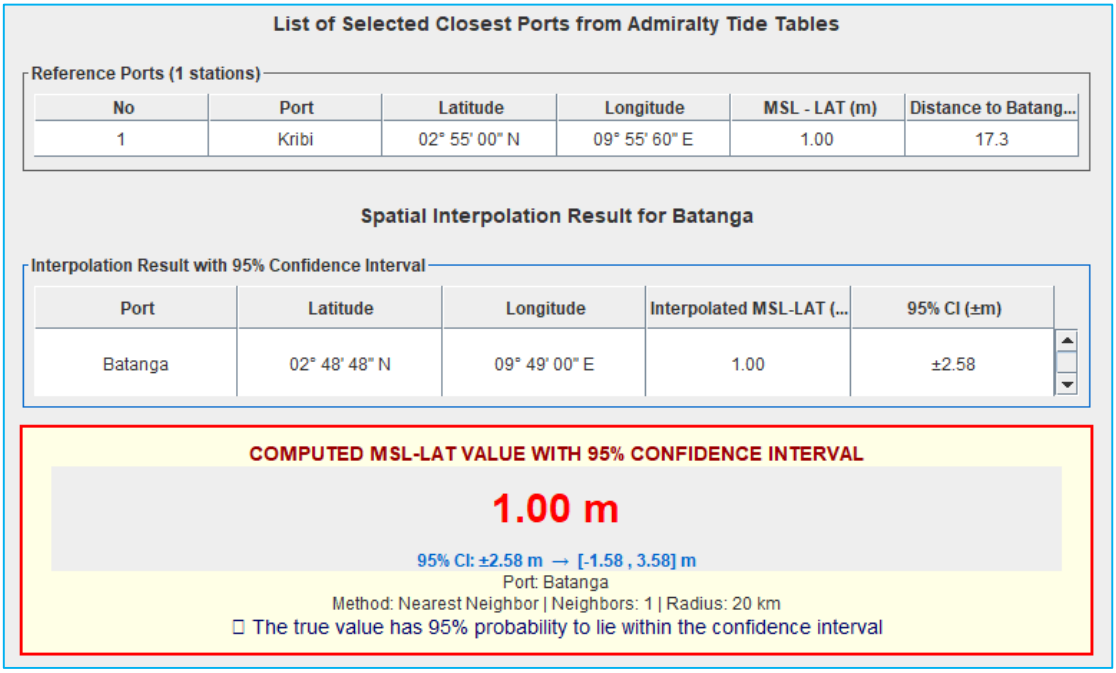

Figure 39. *Spatial interpolation result (NN method) for Batanga: MSL-LAT offset=1.00 m (value from Kribi, nearest station at 17.3 km). Source: LSUHydroTide.*

This is not a spatial interpolation in the strict sense, but a simple proximity assignment. Performance level is unusable in any operational context. A dedicated in-situ tide gauge campaign of at least 15 days is imperative before any professional use.

3.4. Comparative Synthesis of the Three Sites

Table 16 consolidates the characteristics and performances of the three sites.

Table 16. *Characteristics and Comparative Performances of the Three Sites.*

Parameter	Dibamba-Yassa	Betika	Batanga
Context	Wouri Estuary (<20 m)	Rio del Rey Shelf (20-50 m)	Isolated open coast
Available / retained stations	6 / 4	18 / 9	2 / 2
Distance range (km)	16.9 - 50.4	12.2 - 133.0	17.3 - 93.4
Spatial extent (lat × lon)	≈ 0.52° × 0.48°	≈ 1.73° × 2.25°	≈ 0.62° × 0.55°

Parameter	Dibamba-Yassa	Betika	Batanga
Density (st./1,000 km²)	1.766	0.347	0.302
Spatial σ (m) / CV (%)	0.145 / 10.6	0.25 / 18.8	0.16 / 13.8 (n.s.)
Retained method	Trend Surface (kopt=4)	IDW (kopt=9)	NN (default, kopt=1))
MSL-LAT offset (m)	1.571	1.147	1.00
Best RMSE (m)	0.1225 (Trend)	0.2295 (IDW)	0.320 (all)
Best R^2	0.2833 (Trend)	0.1376 (IDW)	-3.000 (all)
σ_t / CI_{95} (m)	±1.834 / ±3.595	±2.479 / ±4.859	±2.375 / ±4.662
Performance level	Good	AccepTable (moderate)	Unusable
Relative confidence (0-3)	2	1-2	0

At Dibamba-Yassa, Trend Surface ranks first (RMSE = 0.1225 m) under favorable conditions of high station density and low variability, while IDW leads at Betika (RMSE = 0.2295 m) despite greater spatial heterogeneity. In both cases, Kriging remains statistically comparable to the leading method, as it consistently ranks second at both Dibamba-Yassa (RMSE=0.1439 m, Δ=0.021 m vs. first) and Betika (RMSE=0.2343 m, Δ=0.005 m vs. first), confirming robustness across contrasted configurations. No meaningful discrimination is possible at Batanga (n=2).

Across all sites, interpolation variance accounts for >95% of total uncertainty regardless of method. A minimum of 5-7 independent stations spaced 20-100 km apart is required for meaningful R^2 and inter-method discrimination. Network densification is therefore the primary operational lever, well ahead of algorithm selection.

Table 17. Method Rankings by Site According to RMSE.

Rank	Dibamba-Yassa (RMSE, m)	Betika (RMSE, m)	Batanga (RMSE, m)
1	Trend (0.1225)	IDW (0.2295)	All (0.320)
2	Kriging (0.1439)	Kriging (0.2343)	-
3	NN (0.1454)	TIN (0.2706)	-
4	TIN (0.1571)	Trend (0.3095)	-
5	Spline (0.1746)	NN (0.3501)	-
6	IDW (0.1777)	Spline (0.3562)	-
RMSE range	0.1225 - 0.1777 (0.055 m)	0.2295 - 0.3562 (0.127 m)	0 (degeneration)

Table 18. Uncertainty Decomposition by Site.

Site	σ_i^2 (m²)	σd² (m²)	σm² (m²)	σ_t (m)	Share σ_i^2 (%)
Dibamba-Yassa (4 st.)	4.4610	0.015 - 0.032	0.006	±1.834	> 95%
Betika (9 st.)	6.0827	0.053 - 0.123	0.010	±2.479	≈ 96%
Batanga (2 st.)	5.5826	0.145	0.003	±2.375	> 98%

3.5. Implications for Operational Hydrography

Interpolated MSL-LAT offsets must be integrated into the total vertical error budget alongside tidal, trajectory, and sounding reduction uncertainties. The 95% CIs (±3.6 m to ±4.9 m) are incompatible with IHO Order 1a tolerances (±0.25 m), mandating either network densification or in-situ tide gauge deployment.

Tables 19 and 20 hierarchise confidence levels and provide methodological recommendations by network density and hydrographic context.

Table 19. Hierarchy of Operational Confidence Levels for the Three Sites.

Site	Context	Reliability	Operational Recommendation
Dibamba-Yassa	Complex estuary (<20 m)	Good	Trend Surface suitable for operational use. In-situ validation by temporary tide gauge (≥15 days) recommended for critical applications.
Betika	Shelf (20-50 m)	Moderate to acceptable	Offshore surveys with conservative vertical margin ≈ ±4.9 m. Densify network to south of site.
Batanga	Isolated open coast	None	Use discouraged without dedicated tide gauge campaign. Nearest station value for indicative use only.

Table 20. Methodological Recommendations by Hydrographic Context and Station Density.

Density / Context	Preferred Method	kopt	Typical RMSE	Operational CI_{95}
≥5-7 stations, extent >1° (Betika, Nigeria/Cameroon clusters)	1-IDW, 2-Kriging, 3-TIN	6-10	0.22-0.29 m	±4.9 m; conservative margins
2-6 stations, extent <0.7° (Dibamba-Yassa, estuaries)	1-Trend, 2-Kriging, 3-NN	2-4	0.12-0.15 m	±3.6 m; in-situ validation required
<3 stations, isolated coast (Batanga, Angola, Guinea)	NN (nearest station)	1	0.32 m	Invalidate; tide gauge campaign required

4. Conclusion

This study systematically compares six spatial interpolation methods for MSL-LAT offset estimation across 115 reference ports in a context of rare and heterogeneous tide gauge data, characteristic of the West African coastline, with application to three Cameroonian test sites representing contrasted hydrographic configurations, using the Java/Swing LSUHydroTide utility.

The main finding is that interpolation quality is governed primarily by the density and geometric configuration of the tide-gauge network, whereas the choice of interpolation algorithm plays a secondary role choice. σ_i^2 consistently represents >95% of the total error budget, creating an operational paradox: accepTable local RMSE (0.165-0.252 m) coexists with 95% CIs of ±3.6 to ±4.9 m.

Methodologically, the best-performing method at Betika was IDW with $k_{opt} = 9$, giving an RMSE of 0.2295 m, $R = 0.1376$, and an estimated MSL-LAT offset of 1.147 m. At Dibamba-Yassa, the Trend Surface method with $k_{opt} = 4$ performed best, with an RMSE of 0.1225 m, $R = 0.2833$, and an estimated offset of 1.571 m. At Batanga, where only two reference stations were available, Nearest Neighbor was the only practicable method, but the leave-one-out result was degenerate and not statistically meaningful; the resulting estimate of 1.000 m must therefore be regarded as indicative only.

Based on three spatial configurations, an empirical minimum of 5-7 independent stations spaced 20-100 km apart is recommended to obtain meaningful R^2 and permit inter-method discrimination. However this threshold should be validated across a broader range of sites. Above this density, geostatistical methods-particularly Ordinary Kriging with a spherical variogram-exhibit strong accuracy and robustness. Kriging consistently ranked second and remained statistically comparable to the top method at Dibamba Yassa and Betika. At Betika, the RMSE gap between Kriging (0.2343 m) and IDW (0.2295 m) is 0.005 m (≈2.1%), a difference negligible given the uncertainty. At

Dibamba-Yassa, Kriging is similarly close to the leader (difference ≈0.011) with a competitive RMSE (0.1439 m) versus the best method (RMSE = 0.1225 m).

Nine complementary GLOSS/PSMSL/UHSLC stations extend spatial coverage northward to 21°N, reducing the main gap in the northern West African domain. Future work should prioritise their in-situ validation to upgrade them to ATT-equivalent primary references, given their current uncertainty of ±0.10-0.15 m derived from harmonic models.

These results lead to a strong recommendation for hydrographic services: priority should be given to densifying and geometrically optimising the regional tide gauge network, notably along southern Cameroon, isolated Angolan sectors, and outer Guinea-Bissau. Betika-type zones can serve as calibration pivots for tidal models. For low-coverage sites, a temporary tide gauge campaign (≥15 days) with GNSS-RTK remains the most effective solution for reducing MSL-LAT uncertainty.

Future work will focus on: (i) hybrid interpolation schemes integrating bathymetric and tidal gradient covariates (co-kriging, adapted TCARI [41]); (ii) coupling with high-resolution hydrodynamic models; (iii) Bayesian probabilistic uncertainty characterisation; and (iv) database extension to southern hemisphere African stations.

Abbreviations

ATT	Admiralty Tide Tables
BLUE	Best Linear Unbiased Estimator
CI	Confidence Interval
GCV	Generalised Cross-Validation
GLOSS	Global Sea Level Observing System
IDW	Inverse-Distance Weighting
IHO	International Hydrographic Organization
JASL	Joint Archive for Sea Level
LAT	Lowest Astronomical Tide
LOO	Leave-One-Out
LOOCV	Leave-One-Out Cross-Validation
MAE	Mean Absolute Error
MSL	Mean Sea Level
NN	Nearest Neighbour
PSMSL	Permanent Service for Mean Sea Level
RMSE	Root Mean Square Error
TCARI	Tidal Constituent and Residual Interpolation
TIN	Triangulated Irregular Network
TPS	Thin-Plate Spline
UHSLC	University of Hawaii Sea Level Center
UTM	Universal Transverse Mercator
WGS84	World Geodetic System 1984

Author Contributions

Michel Mfeze: Conceptualization, Data curation, Formal Analysis, Investigation, Methodology, Resources, Software, Validation, Visualization, Writing – original draft, Writing – review & editing

Data Availability Statement

The data supporting the outcome of this research work has been reported in this manuscript. The full reference-port dataset is provided in Table 1.

Conflicts of Interest

The author declares no conflicts of interest.

References

[1] International Hydrographic Organization. Manual on Hydrography (C-13). Monaco: IHO; 2020. Available from: https://iho.int/uploads/user/pubs/cb/c-13/c-13_ed3-0-0_2020_EN.pdf

[2] Pugh, D., Woodworth, P. Sea-Level Science: Understanding Tides, Surges, Tsunamis and Mean Sea-Level Changes. Cambridge: Cambridge University Press; 2014. https://doi.org/10.1017/CBO9781139235778

[3] Slobbe, D. C., Sumihar, J., Frederikse, T., Verlaan, M., Klees, R., Zijl, F., Farahani, H. H., Broekman, R. A Kalman filter approach to realize the lowest astronomical tide surface. Marine Geodesy. 2018, 41(1), 44-67. https://doi.org/10.1080/01490419.2017.1391900

[4] Erol, B., Erol, S., Çelik, R. N. Height transformation using regional geoids and GPS/levelling in Turkey. Survey Review. 2008, 40(307), 2-18. https://doi.org/10.1179/003962608X253394

[5] Mfeze, M. Harmonic Modeling of Tidal Fluctuations in the Wouri Estuary: A Unified Analysis for Accurate Tide Prediction at the Port Authority of Douala. Journal of Geosciences and Geomatics. 2025, 13(1), 1-22. https://doi.org/10.12691/jgg-13-1-1

[6] United Kingdom Hydrographic Office. Admiralty Tide Tables, Vol. 8: South East Atlantic Ocean, West Africa and Mediterranean (NP208-23). Taunton, UK: UKHO; 2026. Available from: https://www.admiralty.co.uk/publications/publications/admiralty-tide-Tables

[7] W¨oppelmann, G., Marcos, M. Vertical land motion as a key to understanding sea level change and variability. Reviews of Geophysics. 2016, 54(1), 64-92. https://doi.org/10.1002/2015RG000502

[8] Intergovernmental Oceanographic Commission (IOC/UNESCO). Global Sea Level Observing System (GLOSS) Implementation Plan 2022. Paris: IOC/UNESCO; 2022. Available from: https://doi.org/10.25607/OBP-1851

[9] Woodworth, P. L., Hunter, J. R., Marcos, M., Caldwell, P., Menendez, M., Haigh, I. D. Towards a global higher-frequency sea level dataset. Geoscience Data Journal. 2017, 3, 50-59. https://doi.org/10.1002/gdj3.42

[10] Intergovernmental Oceanographic Commission. Manual on Sea Level Measurement and Interpretation, Volume V: Radar Gauges. Paris: IOC/UNESCO; 2017. Available from: https://doi.org/10.25607/OBP-1037

[11] Almar, R., et al. Coastal Zone Changes in West Africa: Challenges and Opportunities for Satellite Earth Observations. Surveys in Geophysics. 2022, 43(1), 249-275. https://doi.org/10.1007/s10712-022-09721-4

[12] Lloyd, C. D. Local Models for Spatial Analysis, 2nd ed. Boca Raton, FL: CRC Press; 2010.

[13] Chilès, J. P., Delfiner, P. Geostatistics: Modeling Spatial Uncertainty, 2nd ed. Hoboken, NJ: Wiley; 2012.

[14] Turner, J. F., Iliffe, J. C., Ziebart, M. K., Wilson, C., Horsburgh, K. J. Interpolation of tidal levels in the coastal zone for the creation of a hydrographic datum. Journal of Atmospheric and Oceanic Technology. 2010, 27(3), 605-613. https://doi.org/10.1175/2009JTECHO645.1

[15] Orton, P., Georgas, S., Blumberg, A., Pullen, J. Detailed modeling of recent severe storm tides in estuaries of the New York City region. Journal of Geophysical Research: Oceans. 2012, 117, C09030. https://doi.org/10.1029/2012JC008220

[16] International Hydrographic Organization. IHO Standards for Hydrographic Surveys: Supplementary Guidance (M-3). Monaco: IHO; 2022. Available from: https://iho.int/uploads/user/pubs/standards/m-3/M-3-Ed2-2.0.0-EN.pdf

[17] Robin, C., Nudds, S., MacAulay, P., Godin, A., De Lange Boom, B., Bartlett, J. Hydrographic vertical separation surfaces (HyVSEPs) for the tidal waters of Canada. Marine Geodesy. 2016, 39(2), 195-222. https://doi.org/10.1080/01490419.2016.1160011

[18] Iliffe, J. C., Turner, J. F., Ziebart, M. K., Talbot, A. J. Ellipsoidal and chart datums in hydrographic surveying: Defining the vertical uncertainty budget. Journal of Navigation. 2013, 66(2), 205-220. https://doi.org/10.1017/S0373463312000537

[19] Li, J., Heap, A. D. Spatial interpolation methods applied in the environmental sciences: A review. Environmental Modelling & Software. 2014, 53, 173-189. https://doi.org/10.1016/j.envsoft.2013.12.008

[20] Matheron, G. Principles of geostatistics. Economic Geology. 1963, 58(8), 1246-1266. https://doi.org/10.2113/gsecongeo.58.8.1246

[21] Guo, J., Hwang, C., Chang, X., Liu, Y. Improved inversion of tide gauge positions from satellite altimetry. Geophysical Research Letters. 2021, 48(5), e2020GL091997. https://doi.org/10.1029/2020GL091997

[22] Kemgang Ghomsi, F. E., et al. Sea level variability in Gulf of Guinea from satellite altimetry. Scientific Reports. 2024, 14(1), 5061. https://doi.org/10.1038/s41598-024-55170-x

[23] African Union Commission. Programme for Africa's Coastal Transformation: Framework for Action (PACT). Addis Ababa: African Union; 2023. Available from: https://au.int/en/documents/20230612/programme-africas-coastal-transformation-framework-action

[24] L. Djeumeni Noubissie, "Sea level variations in the Gulf of Guinea and coastal risks: focus on the Wouri estuary" (in French), Ph.D. dissertation, Université Toulouse III - Paul Sabatier & Université de Douala, 2024.

[25] Idier, D., Castelle, B., Lambert, J., Marieu, V., Pedreros, R. C., Silva, D. A. F. Wave climate and coastal processes along the West African coast. Continental Shelf Research. 2018, 167, 45-60. https://doi.org/10.1016/j.csr.2018.07.004

[26] Reverdin, G., McPhaden, M. J. Seasonal upwelling influence on Gulf of Guinea hydrodynamics. Journal of Physical Oceanography. 2021, 51(6), 1457-1475. https://doi.org/10.1175/JPO-D-20-0256.1

[27] Holgate, S. J., et al. New data systems and products at the Permanent Service for Mean Sea Level. Journal of Coastal Research. 2013, 29(3), 493-504. https://doi.org/10.2112/JCOASTRES-D-12-00175.1

[28] Wöppelmann, G., et al. Dakar sea-level records: 200 years of tide gauge data for sea-level research. SONEL/PSMSL Technical Report; 2008.

[29] Sarr, C. A. T., Ndour, M. M. M., Haddad, M., Sakho, I. Estimation of sea level rise on the West African Coasts: Case of Senegal, Mauritania and Cape Verde. International Journal of Geosciences. 2021, 12(2), 121-137. https://doi.org/10.4236/ijg.2021.122008

[30] Arnould, O., Testut, C. E., Picot, N. Coastal altimetry for tidal analysis in the Gulf of Guinea. Journal of Geophysical Research: Oceans. 2020, 125(8), e2020JC016234. https://doi.org/10.1029/2020JC016234

[31] Sinnott, R. W. Virtues of the haversine. Sky & Telescope. 1984, 68(2), 158-159.

[32] Vincenty, T. Direct and inverse solutions of geodesics on the ellipsoid with application of nested equations. Survey Review. 1975, 23(176), 88-93. https://doi.org/10.1179/sre.1975.23.176.88

[33] Arlot, S., Celisse, A. A survey of cross-validation procedures for model selection. Statistics Surveys. 2010, 4, 40-79. https://doi.org/10.1214/09-SS054

[34] Stone, M. Cross-validatory choice and assessment of statistical predictions. Journal of the Royal Statistical Society: Series B (Methodological). 1974, 36(2), 111-133. https://doi.org/10.1111/j.2517-6161.1974.tb00994.x

[35] Shepard, D. A two-dimensional interpolation function for irregularly-spaced data. In Proceedings of the 1968 ACM National Conference, New York, USA, 1968; pp. 517-524. https://doi.org/10.1145/800186.810616

[36] Bowyer, A. Computing Dirichlet tessellations. The Computer Journal. 1981, 24(2), 162-166. https://doi.org/10.1093/comjnl/24.2.162

[37] Watson, D. F. Computing the n-dimensional Delaunay tessellation with application to Voronoi polytopes. The Computer Journal. 1981, 24(2), 167-172. https://doi.org/10.1093/comjnl/24.2.167

[38] Wahba, G. Spline Models for Observational Data. Philadelphia, PA: Society for Industrial and Applied Mathematics (SIAM); 1990.

[39] Craven, P., Wahba, G. Smoothing noisy data with spline functions: Estimating the correct degree of smoothing by the method of generalized cross-validation. Numerische Mathematik. 1979, 31(4), 377-403. https://doi.org/10.1007/BF01404567

[40] Krige, D. G. A statistical approach to some mine valuation and allied problems on the Witwatersrand. Journal of the Chemical, Metallurgical and Mining Society of South Africa. 1951, 52, 119-139.

[41] Hess, K., Schmalz, R., Zervas, C., Collier, W. Tidal Constituent And Residual Interpolation (TCARI): A New Method for the Tidal Correction of Bathymetric Data. NOAA Technical Report NOS CS 4; 2004. Available from: https://repository.library.noaa.gov/view/noaa/1689

Biography

Michel Mfeze received his Ph.D. in Engineering from the University of Yaounde I, Cameroon, where he is affiliated with the National Advanced School of Engineering of Yaounde (ENSPY). His expertise spans wireless communications (software-defined radio, multipath fading channels, reconfigurable multistandard transceivers) and applied geomatics (GNSS, topographic, hydrographic, and marine geophysical surveys). His geosciences research addresses tidal dynamics, bathymetric and geophysical data processing, spatial interpolation of hydrographic references, and operational hydrography in data-sparse coastal regions, aiming to improve vertical reference systems along the West African coast.

Research Field

Michel Mfeze: Hydrography, Tidal modelling, Vertical reference systems, Spatial interpolation, Geostatistics, Marine geomatics, Coastal dynamics, Geodesy, Bathymetry, Digital Communications, Signal Processing, New radio, Software-defined radio